



**HAL**  
open science

## Complex sporulation-specific expression of transcription termination factor Rho highlights its involvement in *Bacillus subtilis* cell differentiation

Vladimir Bidnenko, Arnaud Chastanet, Christine Péchoux, Yulia Redko-Hamel, Olivier Pellegrini, Sylvain Durand, Ciarán Condon, Marc Boudvillain, Matthieu Jules, Elena Bidnenko

### ► To cite this version:

Vladimir Bidnenko, Arnaud Chastanet, Christine Péchoux, Yulia Redko-Hamel, Olivier Pellegrini, et al.. Complex sporulation-specific expression of transcription termination factor Rho highlights its involvement in *Bacillus subtilis* cell differentiation. 2023. hal-04328824

**HAL Id: hal-04328824**

**<https://hal.science/hal-04328824>**

Preprint submitted on 7 Dec 2023

**HAL** is a multi-disciplinary open access archive for the deposit and dissemination of scientific research documents, whether they are published or not. The documents may come from teaching and research institutions in France or abroad, or from public or private research centers.

L'archive ouverte pluridisciplinaire **HAL**, est destinée au dépôt et à la diffusion de documents scientifiques de niveau recherche, publiés ou non, émanant des établissements d'enseignement et de recherche français ou étrangers, des laboratoires publics ou privés.



Distributed under a Creative Commons Attribution 4.0 International License

1           **Complex sporulation-specific expression of transcription termination factor Rho**  
2           **highlights its involvement in *Bacillus subtilis* cell differentiation.**

3 Vladimir Bidnenko<sup>1\*</sup>, Arnaud Chastanet<sup>1</sup>, Christine Péchoux<sup>2</sup>, Yulia Redko-Hamel<sup>1</sup>, Olivier  
4 Pellegrini<sup>3</sup>, Sylvain Durand<sup>3</sup>, Ciarán Condon<sup>3</sup>, Marc Boudvillain<sup>4</sup>, Matthieu Jules<sup>1</sup>, Elena  
5 Bidnenko<sup>1\*</sup>

6  
7 <sup>1</sup>Université Paris-Saclay, INRAE, AgroParisTech, Micalis Institute, Jouy-en-Josas, France

8 <sup>2</sup>Université Paris-Saclay, INRAE, AgroParisTech, GABI, Jouy-en-Josas, France

9 MIMA2 Imaging Core Facility, Microscopie et Imagerie des Microorganismes, Animaux et  
10 Aliments, INRAE, Jouy-en-Josas, France

11 <sup>3</sup>Expression Génétique Microbienne, UMR8261 CNRS, Université Paris Cité, Institut de  
12 Biologie Physico-Chimique, Paris, France.

13 <sup>4</sup>Centre de Biophysique moléculaire, CNRS UPR4301, Orléans, France; affiliated with  
14 Université d'Orléans, France

15  
16  
17  
18  
19  
20  
21 \* Co-corresponding authors

22

23

24

25

26

27

28

29

30

31

## 32 **Abstract**

33

34 Transcription termination factor Rho controls pervasive, mainly antisense, transcription  
35 initiated at cryptic signals or resulting from read-through at weak terminators in various  
36 bacterial species. In *Bacillus subtilis*, Rho is intricately involved in the regulation of  
37 phenomena associated with the adaptation to stationary phase and cell differentiation including  
38 the ultimate survival program of sporulation.

39 While knockout or overexpression of the *rho* gene alters global transcription and modifies cell  
40 physiology, in wild-type *B. subtilis* cells, the reduction of Rho levels during the transition to  
41 stationary phase is necessary for both initiation and implementation of the sporulation program.  
42 However, the mechanisms that govern Rho expression throughout the cell cycle remain largely  
43 unknown.

44 Here, we demonstrate that, besides the previously identified vegetative SigA-dependent  
45 promoter active during exponential growth, two distinct mechanisms ensure a spatiotemporal  
46 expression of the *rho* gene during sporulation. In the mother cell of the sporangium, *rho*  
47 expression occurs through the read-through transcription initiated at the distal SigH-dependent  
48 and Spo0A~P-regulated promoter of the *spo0F* gene. In the forespore, *rho* is transcribed from  
49 a genuine promoter recognized by the alternative sigma factor SigF. These regulatory elements  
50 compensate for the inactivation of SigA-dependent *rho* expression at the end of exponential  
51 growth and allow the critical “refueling” of Rho protein in both compartments of the  
52 sporangium. We show that altering *rho* expression in the mother cell or in the forespore affects  
53 differently the properties and the morphology of mature spores. Moreover, spores formed in the  
54 absence of Rho are impaired in their ability to revive under favorable growth conditions,  
55 exhibiting accelerated germination and slow outgrowth. Finally, we show that optimal  
56 outgrowth of the wild-type spores requires the expression of *rho* during spore maturation and  
57 additionally after spore germination.

58

59

## 60 **Introduction**

61

62 A growing understanding of the importance of transcription termination in the regulation of  
63 gene expression in bacteria has stimulated extensive analysis of the proteins that control this  
64 universal step in decoding genetic information (Peters et al., 2011; Ray-Soni et al., 2016; Kriner

65 et al., 2016; Turnbough, 2019; Mandell et al., 2022a). Among them is transcription termination  
66 factor Rho, an ATP-dependent RNA helicase-translocase that improves the termination  
67 efficiency of many intrinsic terminators and is essential for termination at bona-fide Rho-  
68 dependent terminators (Roberts, 1969; Quirk et al., 1996; Peters et al., 2009; Hao et al., 2021;  
69 Mandell et al., 2022b). Over the last years, considerable advances have been made in unveiling  
70 the molecular mechanism of Rho-dependent termination (Song et al., 2022; Molodtsov et al.,  
71 2023; Murayama et al., 2023; Rashid and Berger, 2023).

72 Transcriptome analyses of *rho* knockout and conditionally deficient mutants of various bacteria  
73 have established the essential role of Rho in controlling pervasive, mainly non-coding and  
74 antisense, transcription that originates from cryptic initiation signals or from read-through of  
75 transcription terminators (Nicolas et al., 2012, Peters et al., 2012; Mäder et al., 2016; Botella et  
76 al, 2017). By controlling transcription genome-wide, Rho directly and indirectly influences  
77 various aspects of cellular physiology in bacteria living in diverse habitats (Bidnenko et el.,  
78 2017, 2023; Botella et al., 2017; Nagel et al., 2018; Trzilova et al., 2020; Lin et al.; 2021;  
79 Kryptou et al., 2023). It is notable that Rho is involved in the regulation of phenomena  
80 associated with stationary phase, including stress survival, cell fate determination, antibiotic  
81 sensitivity, host colonization and virulence in different bacteria (Lee and Helmann, 2014; Liu  
82 et al., 2016; Hafeezunnisa et al., Bidnenko et al., 2017, 2023; Nagel et al., 2018; Trzilova et al.  
83 2020; Lin et al., 2021; Figueroa-Bossi et al., 2022).

84 Recently, we provided evidence that Rho is intricately involved in the control of cellular  
85 adaptation to stationary phase and in cell-fate decision-making, in particular, the decision to  
86 sporulate, in the Gram-positive bacterium *Bacillus subtilis* (Bidnenko et al., 2017, 2023). The  
87 involvement of Rho in the sporulation process was also demonstrated in *Clostridioides difficile*  
88 and *Bacillus thuringiensis* (Trzilova et al., 2020; Lin et al.; 2021).

89 Sporulation is a complex developmental program that transforms a vegetative bacterial cell into  
90 a highly resistant dormant spore, thus ensuring the survival of bacteria under adverse  
91 environmental conditions and their dissemination within different ecological niches (de Hoon  
92 et al., 2010; Swick et al., 2016; Galperin et al., 2022). A hallmark of sporulation in *B. subtilis*  
93 is the asymmetric division of a differentiating cell in two unequal parts: a forespore, which  
94 further develops into the spore, and a mother cell, which engulfs the forespore, nourishes it,  
95 ensures the synthesis of spore protective layers, and finally lyses to release the mature spore.  
96 Proper spore morphogenesis is essential for spore resistance to external damages and its  
97 conversion back into a growing cell under favorable conditions through sequential processes of

98 germination and outgrowth (Setlow, 2003; Setlow et al., 2017; Setlow and Christie, 2023;  
99 Segev et al., 2013; Abhyankar et al., 2016; Boone and Driks, 2016; Mutlu et al., 2018; 2020).  
100 In *B. subtilis*, sporulation is primarily controlled at the level of transcription initiation by the  
101 master regulator Spo0A, whose activity depends on phosphorylation mediated by a multi-  
102 component phosphorelay, the transition phase-specific sigma factor SigH and a cascade of  
103 sigma factors (SigF, SigE, SigG and SigK) that sequentially drive temporally- and spatially-  
104 defined transcriptional programs of spore morphogenesis. Sporulation is initiated at a threshold  
105 level of Spo0A~P, which activates the expression of *sigH* and several sporulation genes,  
106 including *sigF* and *sigE* encoding the inactive forms of sigma factors. Upon completion of the  
107 asymmetric septum, activation of SigF in the forespore is required for subsequent activation of  
108 SigE in the mother cell. After a complete engulfment of the forespore, the compartment-specific  
109 programs of gene expression are further continued by SigG in the forespore and SigK in the  
110 mother cell (for comprehensive reviews see Errington, 1993; Stragier and Losick, 1996; Piggot  
111 and Hilbert, 2004; Higgins and Dworkin, 2012). The relevant regulons of each sporulation-  
112 specific sigma factor, as well as other genes involved in sporulation, were determined using the  
113 combination of experimental and bioinformatics approaches (Eichenberger et al., 2003, 2004;  
114 Steil et al., 2005; Wang et al., 2006; de Hoon et al., 2010; Overkamp et al., 2015; Meeske et al.,  
115 2016; Galperin et al., 2022).

116 We have previously shown that deletion of the *rho* gene in *B. subtilis* prevents intragenic  
117 termination of the *kinB* transcript, which encodes the sensor kinase KinB, one of the main  
118 kinases feeding phosphate into the Spo0A phosphorelay. This leads to the increased expression  
119 of KinB and, consequently, to rapid accumulation of active Spo0A~P to a threshold level that  
120 triggers sporulation. Thus, Rho inactivation stimulates sporulation in *B. subtilis* indicating a  
121 regulatory role of Rho-mediated transcription termination within the cell fate decision-making  
122 network centered on Spo0A~P (Bidnenko et al., 2017). Conversely, maintaining *rho* expression  
123 at a stably elevated level throughout *B. subtilis* exponential growth and stationary phase alters  
124 the early steps of adaptive reprogramming of cellular transcription, prevents the activation of  
125 Spo0A and, additionally, inhibits some late, yet non-identified, sporulation events, with the  
126 overall result of blocking the formation of spores (Bidnenko et al., 2023).

127 Comparative transcriptome and proteome analyses have revealed a decrease in the levels of *rho*  
128 mRNA and Rho protein during the transition to stationary phase in wild-type *B. subtilis* cells  
129 (Nicolas et al., 2012; Bidnenko et al., 2017; 2023). Considering that Rho negatively affected  
130 sporulation in our analyses, a decrease in Rho levels appears necessary for both initiation and

131 implementation of the sporulation program. This in turn suggests that *rho* expression during *B.*  
132 *subtilis* growth and stationary phase is subject to reliable and timely regulation.

133 The only mechanism known to date for regulating *rho* expression is transcriptional attenuation  
134 at the Rho-dependent terminator(s) located within the leader region of the *rho* transcript and  
135 consequent premature transcription termination (Ingham et al., 1999). Similar to *B. subtilis*,  
136 transcription of the *rho* gene was shown to be autogenously regulated in *Escherichia coli*,  
137 *Salmonella* and *Caulobacter crescentus* (Barik et al., 1985; Matsumoto et al., 1986; Italiani et  
138 al., 2005; Silva et al., 2019). In *Salmonella*, *rho* autoregulation is counteracted by the small  
139 noncoding RNA SraL, which prevents the Rho-mediated termination by direct binding the 5'-  
140 UTR of *rho* mRNA (Silva et al., 2019).

141 In the present study, we aimed to gain further insights into *rho* regulation in *B. subtilis* by  
142 analyzing the kinetics of *rho* expression at various stages of cellular growth and differentiation.  
143 Quite unexpectedly, we found that the expression of the *rho* gene is specifically induced early  
144 during sporulation. This counterintuitive finding has focused our subsequent analysis on  
145 understanding the mechanism of the sporulation-specific expression of *rho* and its biological  
146 significance.

147 We describe two distinct mechanisms controlling *rho* expression in each compartment of the  
148 sporulating cells: read-through transcription from the upstream SigH-dependent promoter in the  
149 mother cell, and a genuine SigF-dependent *rho* promoter active in the forespore. The latter  
150 feature allows us to classify *rho* as a novel member of the SigF regulon of *B. subtilis*. We  
151 provide evidence that altering the spatiotemporal expression of *rho* affects spore resistance  
152 properties and morphology, in particular, the structure of spore coat. Moreover, spores formed  
153 in the absence of Rho are impaired in their ability to revive under favorable growth conditions,  
154 exhibiting an accelerated germination and a slow outgrowth. Finally, we show that the optimal  
155 rate of spore outgrowth depends on the synthesis of Rho during spore formation and *de novo*  
156 after germination.

157

## 158 **Results**

159

### 160 **Rho expression is specifically induced during sporulation.**

161 To analyze a real-time expression of the *rho* gene, we constructed a scarless reporter system, in  
162 which the luciferase gene *luc* of firefly *Photinus pyralis* was fused to the *rho* promoter ( $P_{rho}$ ) at

163 the position of the *rho* start codon. The P<sub>*rho*</sub>-*luc* fusion was similarly located in the *rho* locus of  
164 the chromosome in the wild type *B. subtilis* strain BSB1 and the *rho* deletion mutant RM  
165 (Bidnenko et al., 2017). The former strain (hereinafter WT) kept an active copy of the *rho* gene  
166 due to duplication of the *rho* locus during the construction. By comparing luciferase activity in  
167 WT and RM strains under different growth conditions, we sought to assess Rho autoregulation  
168 and possibly identify other regulatory factors.

169 In WT cells grown in rich medium LB, the expression of *rho* was mainly limited to the  
170 exponential growth phase, characterized by two peaks of luciferase activity at OD<sub>600</sub> ~0.15 and  
171 ~0.4 (Fig 1A). In stationary phase, *rho* expression remained at a basal level. A low-level  
172 expression of *rho* and its down-regulation during the transition to stationary phase were  
173 reported previously (Ingham et al., 1999; Nicolas et al., 2012; Bidnenko et al., 2017; 2023).  
174 The inactivation of Rho in RM cells did not alter the kinetics of *rho* expression, but rather  
175 increased its level approximately threefold, suggesting a release from autoregulation (Fig 1A).  
176 WT cells grown in the sporulation-promoting Difco Sporulation Medium (DSM) showed a  
177 different *rho* expression kinetics, characterized by the additional peak of luciferase activity in  
178 stationary phase (Fig 1B). The reactivation of *rho* expression coincided in time with the  
179 induction of the sporulation-specific *spoIIAA-AB-sigF* operon, monitored in a separate strain  
180 using the P<sub>*spoIIAA*</sub>-*luc* transcriptional fusion (Fig 1B; Bidnenko et al, 2017). The similarity in  
181 timing suggested that *rho* expression during stationary phase in DSM might be linked to  
182 sporulation.

183 In RM cells grown in DSM, luciferase activity increased ~7-fold compared to WT cells during  
184 exponential growth, but only ~1.5-fold in stationary phase. This suggests that *rho* expression in  
185 stationary phase is not subject to significant autoregulation. Curiously, however, the stationary  
186 phase-specific expression of *rho* was activated considerably earlier in RM than in WT cells (Fig  
187 1C). This effect was reminiscent of the accelerated expression of *spo0A* gene in the sporulating  
188 RM cells caused by the up-regulation of Spo0A phosphorelay (Bidnenko et al., 2017).  
189 Therefore, we compared the expression of *rho* and *spo0A* genes in WT and RM cells grown in  
190 DSM using the P<sub>*rho*</sub>-*luc* and P<sub>*spo0A*</sub>-*luc* fusions (Mirouze et al., 2012; Bidnenko et al., 2017). In  
191 both strains, *rho* expression in stationary phase timely followed *spo0A* and, in RM cells, the  
192 maximal expression levels of both genes was reached ~1.5 hour earlier than in WT (Fig 1D).  
193 This observation additionally argued for the sporulation-specific expression of *rho* as a function  
194 of Spo0A~P activity.

195 To get more insights into the sporulation-specific expression of *rho*, we analyzed the P<sub>*rho*</sub>-*luc*  
196 activity in *B. subtilis* sporulation mutants. First, we considered *spo0A* and *sigH* mutations,

197 which block initiation of sporulation by inactivating Spo0A and the transition phase-specific  
198 sigma factor SigH, respectively. Neither *spo0A* nor *sigH* mutations affected  $P_{rho}$ -*luc* activity  
199 during exponential growth in DSM, but both specifically blocked it in stationary phase, thus  
200 confirming that *rho* expression at this stage is dependent on sporulation-specific factors (Fig  
201 1E).

202 Next, we assessed the involvement of the alternative SigF and SigE factors controlling early  
203 gene expression in the forespore and mother cell, respectively. The kinetics of  $P_{rho}$ -*luc* activity  
204 in *sigF* and *sigE* mutants was rather similar to WT cells. However, the stationary phase-specific  
205 luminescence appeared slightly lower in the *sigF* background and, in both mutants, remained  
206 high after reaching a maximal level (Fig 1F). These results indicated some deregulating effects  
207 of *sigF* and *sigE* mutations and suggested that *rho* is expressed in both compartments of  
208 sporulating cells.

209 Considering that the known SigA-controlled  $P_{rho}$  promoter is mainly active during exponential  
210 growth (Fig 1A), we sought for additional regulatory factors of *rho* expression during  
211 sporulation.

212

### 213 **The read-through transcription from the upstream SigH-controlled promoter** 214 **contributes to *rho* expression during sporulation.**

215 The *rho* gene is transcribed from the cognate  $P_{rho}$  promoter together with the upstream non-  
216 coding S1436 element and the downstream *rpmE* gene in a transcript of ~1.9 kb (Quirk et al.,  
217 1991; Ingham et al., 1999; Nicolas et al., 2012). Additionally, the genome-wide transcriptome  
218 analyses have revealed several longer read-through transcripts at the *rho* locus, which initiate  
219 at the upstream *spo0F* and *fbaA-ywjH* promoters and bypass the intrinsic terminators of the  
220 *ywjH* and *glpX* genes (Nicolas et al., 2012; Mandell et al., 2022b; Fig 2A).

221 We asked whether read-through transcription could play a role in the expression of *rho*, in  
222 particular during sporulation, as *spo0F* gene is known to be transcribed from alternative SigA-  
223 and SigH-dependent promoters, with the latter also being regulated by Spo0A~P (Lewandoski  
224 et al., 1986; Predich et al., 1992; Strauch et al., 1993; Asayama et al., 1995). To this end, we  
225 sought to enhance transcription termination upstream of the *rho* gene and inserted a DNA  
226 fragment containing three intrinsic transcription terminators after the stop codon of the *glpX*  
227 gene (hereafter referred 3Ter; Fig 2B; Vagner et al., 1998; Bidnenko et al., 2017). To assess  
228 read-through transcription at the *rho* locus and the termination efficiency of the 3Ter insertion,  
229 we analyzed *rho*-specific transcripts in WT, *sigH* and 3TER mutant cells by Northern blot (Fig

230 2C). Cells were grown in DSM and sampled during exponential growth (OD<sub>600</sub> 0.5), transition  
231 phase (OD<sub>600</sub> 1.0) and in stationary phase, at OD<sub>600</sub> 1.8. In WT and *sigH* mutant cells, we  
232 observed several *rho*-specific RNA species, the smallest and most abundant of which  
233 corresponded in size to the 1.9 kb *rho-rpmE* mRNA, and the largest (~7 kb) to transcripts  
234 initiated at the *fbaA* and/or *spo0F* promoters. Other RNAs of ~4-5 kb in size cannot be assigned  
235 to any defined promoter and may result from ribonuclease processing of the larger transcripts.  
236 During transition to stationary phase, the larger *rho*-specific RNAs accumulated in WT cells,  
237 but gradually disappeared in *sigH* mutant, in accordance with the notion that *spo0F*  
238 transcription in stationary phase depends on SigH activity (Fig 2C). Notably, none of the larger  
239 *rho*-specific transcripts were detectable in 3TER cells (Fig 2C) confirming that they do indeed  
240 originate from upstream of the inserted terminators. All together, these results show an efficient  
241 read-through transcription of the *rho* gene, mainly initiated at the *spo0F* promoter.

242 Northern analysis also provided information about P<sub>*rho*</sub> functioning. The levels of the 1.9 kb *rho*  
243 transcript decreased in stationary WT cells, in line with the down-regulation of the SigA-  
244 dependent P<sub>*rho*</sub> at this stage (Fig 2C; Nicolas et al., 2012), and became barely detectable in the  
245 stationary *sigH* mutant cells (Fig 2C). However, the dramatic decrease in the abundance of this  
246 short transcript in the *sigH* mutant was not due to the inhibition of read-through transcription  
247 from P<sub>*spo0F*</sub> promoter, as the amount of the 1.9 kb *rho* transcript remained high in the stationary  
248 3TER cells (Fig 2C).

249 To better understand the expression of *rho* in the absence of read-through transcription, we  
250 analyzed the activity of P<sub>*rho*</sub>-*luc* fusion in the 3TER strain and its sporulation-deficient  
251 derivatives. In 3TER P<sub>*rho*</sub>-*luc* cells grown in DSM, luciferase activity was identical to WT P<sub>*rho*</sub>-  
252 *luc* during exponential growth, but decreased ~3-fold in stationary phase, highlighting the role  
253 of read-through transcription in the *rho* expression at this stage (Fig 2D). Intriguingly, the  
254 residual luminescence in the stationary 3TER P<sub>*rho*</sub>-*luc* cells was blocked by *spo0A* and *sigH*  
255 (Fig 2E) and partially inhibited by *sigF* inactivation, while mutation of *sigE* had no effect (Fig  
256 2F). All together, these results indicated that the *glpX-rho* intergenic region contains additional  
257 structural factor(s) of *rho* expression active during sporulation and likely dependent on SigF.

258

### 259 **The sporulation-specific expression of *rho* is compartmentalized.**

260 Since SigF is primarily associated with the forespore, this led us to investigate potential  
261 compartmentalization of *rho* expression during sporulation. To this end, we constructed a P<sub>*rho*</sub>-  
262 *gfp* fusion expressing green fluorescent protein GFP at the *rho* chromosomal locus of WT cells

263 and analyzed its activity during sporulation at a single-cell level by fluorescence microscopy.  
264 We observed an increase of fluorescence intensity in the forespores of the sporulating WT  $P_{rho}$ -  
265 *gfp* cells immediately after asymmetric division (S1 Fig and Fig 3). This observation further  
266 suggested a particular role of SigF in the sporulation-specific expression of *rho*. Following it,  
267 we analyzed the activity of  $P_{rho}$ -*gfp* fusion in *sigF* and *sigE* mutant cells.  
268 Absence of SigE disables the SigE-dependent inhibitors of septation, therefore provoking the  
269 formation of asymmetric septa at both poles of sporulating cells (Illing and Errington, 1991;  
270 Setlow et al., 1991; Lewis et al., 1994; Eichenberger et al., 2001). Because activation of SigE  
271 in the mother cell sequentially depends on SigF activity in the forespore (Londono-Vallejo &  
272 Stragier, 1995; and references therein), both *sigE* and *sigF* mutants display a similar disporic  
273 cell phenotype. Such disporic cells were readily seen in  $P_{rho}$ -*gfp sigF* and  $P_{rho}$ -*gfp sigE*  
274 sporulating cultures, in addition to cells containing one asymmetric septum. The mother cells  
275 of both *sigF* and *sigE* sporangia maintained GFP signal at a level similar to that of WT,  
276 indicating that *rho* expression is SigE-independent (Fig 3). In contrast, while the forespore-like  
277 structures showed an increased fluorescence in *sigE* mutant similarly to the WT forespores,  
278 their brightness was significantly diminished in *sigF* sporangia (Fig 3). Together with the results  
279 from the previous section, this observation indicated that, in forespores, *rho* is expressed from  
280 a promoter located in the *glpX-rho* intergenic region and dependent, directly or indirectly, on  
281 SigF.

282

### 283 **The 5'-UTR of *rho* contains a genuine SigF-dependent promoter active in forespores.**

284 Previous analyses have identified a *rho* promoter that matches the SigA-binding sequence  
285 consensus ( $^{sigA}P_{rho}$ ) 293-320 bp upstream the *rho* start codon (Quirk et al., 1993; Ingham et al.,  
286 1999; Fig 4A). Recent reassessment of *B. subtilis* promoters using the unsupervised sequence  
287 clustering algorithm has classified  $^{sigA}P_{rho}$  to the M16 cluster of SigA-dependent promoters,  
288 which are characterized by an extended 3'-terminal G-rich -10 box and a variable -35 box with  
289 the conserved TTG stretch (Nicolas et al., 2012; Fig 4B). Looking for alternative *rho*  
290 expression signals, we analyzed the *glpX-rho* intergenic region for the presence of the SigF-  
291 binding consensus -35 (GYATA) and -10 (GGnnAnAHTR) sequences, where Y is C or T; H is  
292 A or C or T; R is A or G; and n is any nucleotide (Wang et al., 2006). Such features were found  
293 within the  $^{sigA}P_{rho}$  sequence itself (Fig 4C). Within the -10 box of  $^{sigA}P_{rho}$ , we identified  
294 GGTA AAAATA sequence perfectly matching the SigF -10 consensus and, 14 bp upstream, a  
295 5-nucleotide GAATA sequence differing from the SigF -35 consensus by one nucleotide. Of

296 note, the same -35 sequence is present in the SigF-regulated promoters of *yuiC*, *yabT*, *yjbA*,  
297 *ypfB* and *ythC* genes (Wang et al., 2006). Moreover, the 14-bp spacer between -35 and -10  
298 sequences is highly A/T-rich that is characteristic of most SigF-dependent promoters (Wang et  
299 al., 2006).

300 To prove that the identified sequences constitute a novel SigF-dependent *rho* promoter  
301 (hereafter  $\text{sig}^F\text{P}_{rho}$ ), we proceeded to site-directed mutagenesis of the  $\text{P}_{rho-gfp}$  fusion, anticipating  
302 that altering the SigF-binding sequences would specifically affect GFP expression in the  
303 forespores. Because of a strong overlap between the -10 sequences of  $\text{sig}^A\text{P}_{rho}$  and putative  
304  $\text{sig}^F\text{P}_{rho}$ , we targeted the -35 GAATA sequence of the latter and replaced the invariant T  
305 nucleotide (Amaya et al., 2001; Wang et al., 2006) with A (*mF-35T/A P<sub>rho-gfp</sub>*) or C (*mF-35T/C*  
306 *P<sub>rho-gfp</sub>*) (Fig 4C). Next, we compared the activity of the mutant fusions with the original one  
307 (WT *P<sub>rho-gfp</sub>*) and the one preceded by the transcriptional terminators (3TER *P<sub>rho-gfp</sub>*). Cells  
308 were set to sporulate in DSM medium, and the fluorescence levels in predivisional cells and  
309 two compartments of sporangia were quantified at the time of a maximal SigF activity. As we  
310 observed earlier (Fig 3), the sporulating WT *P<sub>rho-gfp</sub>* cells showed a higher level of fluorescence  
311 in the forespores than in the mother cells; in the latter, *gfp* expression appeared similar to  
312 predivisional cells confirming our hypothesis that *rho* expression in the mother cell is SigE-  
313 independent (Fig 4D and 4E). A similar pattern of the brighter forespores was observed in 3TER  
314 *P<sub>rho-gfp</sub>* cells, even though the fluorescence was globally lower probably due to the inhibition  
315 of the read-through transcription by the 3Ter insert (Fig 4D and 4E).

316 In contrast, and as expected, both *mF-35T/A* and *mF-35T/C* mutations of *P<sub>rho-gfp</sub>* specifically  
317 inhibited the burst of fluorescence in the forespores, similarly to *sigF* mutation (Fig 4D and  
318 4E, and Fig 3). At present, it is unclear why *mF-35T/A P<sub>rho-gfp</sub>* mutant strain displayed a higher  
319 basal fluorescence (Fig 4E). Nevertheless, these results clearly indicate that the forespore-  
320 specific expression of *rho* depends on the alternative promoter  $\text{sig}^F\text{P}_{rho}$ .

321 This conclusion was further supported by the analysis of the mutated *P<sub>rho-luc</sub>* fusion: both point  
322 mutations *mF-35T/A* and *mF-35T/C* efficiently inhibited the sporulation-specific luciferase  
323 activity in 3TER cells (S2 Fig).

324 Overall, our results indicate that, during growth and sporulation, the expression of *rho* gene  
325 relies on three distinct features: (i) a SigA-dependent *rho* promoter that is active during  
326 exponential growth, (ii) read-through transcription from the upstream SigH-dependent *spo0F*  
327 promoter during early stationary phase and in the mother cells of sporangia, and (iii) a SigF-  
328 dependent *rho* promoter active in the forespores.

329

### 330 **Differential expression of Rho affects spore properties and morphology.**

331 The revealed spatiotemporal expression of *rho* suggested that besides modulation of Spo0A  
332 activity at the onset of sporulation (Bidnenko et al., 2017), Rho can be involved in the  
333 subsequent steps of spore development. To address this hypothesis, we used a set of five strains  
334 differentially expressing Rho during sporulation, namely: the wild type (WT), a strain blocked  
335 for the *rho* read-through transcription (3TER), their derivatives inactivated for *rho* expression  
336 in the forespore by *mF-35T/A* mutation of  $\text{sig}^{\text{F}}\text{P}_{rho}$  (WT-mT/A and 3TER-mT/A), and a mutant  
337 deleted for *rho* (RM).

338 Initially, we compared sporulation capacities of the five strains. To this end, we induced  
339 sporulation by the resuspension method and assessed asymmetric division of individual cells  
340 and formation of the heat-resistant spores at the initial and final stages of sporulation,  
341 respectively. Among the five strains, RM cells showed a highest rate of asymmetric division  
342 corroborating our previous data on the accelerated sporulation of  $\Delta rho$  mutant, most probably  
343 due to a more efficient activation of Spo0A (S3 Fig; Bidnenko et al., 2017). Interestingly, the  
344 proportion of cells with asymmetric septum was also higher in 3TER and 3TER-mT/A strains  
345 compared to WT or WT-mT/A mutant (S3 Fig) suggesting a regulatory crosstalk between  
346 Spo0A~P activating read-through transcription of *rho* and Rho modulating activity of the  
347 Spo0A phosphorelay. However, while RM formed the heat-resistant spores considerably faster  
348 and with maximal yield, other mutants resembled more WT cells (S3 Fig). Therefore, only the  
349 complete inactivation of Rho significantly affected sporulation dynamics.

350 Next, we let cells to sporulate in DSM for 24 hours, during which more than 80 percent of cells  
351 in each strain formed spores, purified the mature spores, and compared some of their damage  
352 resistance properties. It should be noted, however, that most resistance phenotypes of spores  
353 are determined by multifactorial mechanisms, what makes their dissection difficult (reviewed  
354 in Setlow, 2006; Setlow and Christie, 2023). All spores differentially expressing *rho* were  
355 similarly resistant to lysozyme, which targets the cortex peptidoglycan (reviewed in Henriques  
356 and Moran, 2007), and became similarly sensitive to it after chemical removal of the coat (S4  
357 Fig). This indicates that the permeability of spore coat to lysozyme was not detectably affected  
358 by altered expression of *rho*. Likewise, all five types of spores showed similar levels of wet-  
359 heat resistance, a complex spore phenotype determined by factors expressed in both spore  
360 compartments (S4 Fig). At the same time, unlike the others, RM spores contained higher  
361 (~35%) levels of dipicolinic acid (DPA) (Fig 5A), an important factor of the heat-resistance

362 synthesized in the mother cell, but accumulated in the spore core (reviewed in Nicholson et al.,  
363 2000; Setlow, 2016). Moreover, the mutant RM and also WT-mT/A and 3TER-mT/A spores,  
364 formed in the absence of the forespore-specific expression of *rho*, appeared more sensitive to  
365 ultraviolet (UV) light than WT and 3TER spores (Fig 5B). This effect was spore-specific, as  
366 vegetative RM and WT cells were equally resistant to UV radiation (S5 Fig). The UV-resistance  
367 of mature spores is mainly determined by the  $\alpha/\beta$  small acid-soluble proteins (SASPs) and  
368 photoproduct lyase SplB synthesized in the forespores (Mason and Setlow, 1986; Pedraza-  
369 Reyes et al., 1994; Setlow, 2007). Based on our results, it is possible that Rho expressed from  
370 SigF-dependent promoter is involved in the regulation of some of these UV-resistance factors.  
371 Finally, we analyzed the ultra-structure of the purified spores by transmission electron  
372 microscopy, which revealed significant differences between the spores in the structure of their  
373 coats (Fig 6). In accordance with numerous previous studies (reviewed in Henriques & Moran,  
374 2007; McKenney et al., 2013; Driks and Eichenberger, 2016), WT spores exhibited a regular  
375 surface layer composed of a lamellar inner coat and a striated thick electron-dense outer coat.  
376 Two coats were tightly attached to each other in a large majority (over 92 percent) of WT spores  
377 or occasionally separated across a limited area (Fig 6). In contrast, RM spores contained a  
378 lamellar inner coat similar to WT spores, but their outer coat remarkably lost electron-density  
379 and striated structure and appeared half thinner compared to WT spores (respectively, 36.2 +/-  
380 0.0091 nm and 74.2 +/- 0.021 nm, as measured for 100 spores of each strain). Moreover, above  
381 80 percent of RM spores showed an extensive detachment of inner and outer coats, often along  
382 the entire spore perimeter (Fig 6). Spores differentially expressing *rho* exhibited intermediate  
383 ranges of structural alterations of their coats. The outer coat of 3TER spores appeared less  
384 striated and low electron-dense compared to WT, therefore resembling the RM coat. Moreover,  
385 the outermost layer often peeled off the 3TER spore surface. However, we did not observe  
386 3TER spores with the separated inner and outer coats (Fig 6). In WT-mT/A spores, the outer  
387 coat was electron-dense and striated like a WT layer, but detached from the inner coat in ~30  
388 percent of spores, although across less extended areas than in RM spores (Fig 6). Finally, 3TER-  
389 mT/A spores contained a low structured outer coat locally separated from the inner coat in ~30  
390 percent of spores (Fig 6). By combining these features, 3TER-mT/A spores appear most similar  
391 to RM spores, which seems in line with the absence of sporulation-specific *rho* expression in  
392 both mutant strains. We conclude that altering expression of *rho* during sporulation in the  
393 mother cell (3TER) or in the forespore (mT/A) induces specific defects of spore morphology,  
394 which are accentuated by the entire loss of the Rho activity in RM strain.

395

396 **Rho mediates spore germination and outgrowth.**

397 The ability to resume vegetative growth in favorable nutrient conditions, referred to as spore  
398 revival, is a basic spore property and spore quality indicator (Henriques and Moran, 2007;  
399 Setlow, 2013; Sinai et al, 2015; Ramírez-Guadiana et al., 2017a; Christie and Setlow, 2020).  
400 We compared the revival abilities of spores differentially expressing Rho by evaluating the  
401 optical density (OD<sub>600</sub>) of spore suspensions after the induction of germination. Rapid  
402 rehydration and structural changes of the germinating spores alter their optical properties  
403 resulting in a decrease in OD<sub>600</sub>. The OD<sub>600</sub> of reviving spores remains stable during the post-  
404 germination phase of metabolic resumption and molecular reorganization, designated the  
405 “ripening period”, before increasing later during spore outgrowth, when the emerging cells  
406 start to grow and divide (Segev et al., 2013; Rosenberg et al., 2015). For simplicity, we  
407 consider the outgrowth period as a time needed for a spore culture to restore its initial OD<sub>600</sub>  
408 after germination.

409 After the addition of the germinant L-alanine, RM spores lost OD<sub>600</sub> faster than the others, thus  
410 showing the highest germination rate (Fig 7A). Similarly, RM spores germinated more  
411 efficiently with the germinants AGFK (a mixture of L-asparagine, glucose, fructose and  
412 potassium chloride) and L-valine recognized by other germinant receptors than L-alanine (S6  
413 Fig). Other spores germinated similarly to WT with all three germinants (Fig 7A and S6 Fig).  
414 In contrast to the rapid germination, the outgrowth of RM spores in a defined minimal medium  
415 was significantly delayed compared to other spores (Fig 7B). At the same time, the viability of  
416 RM spores during germination was not decreased compared to WT spores (S7 Fig) and  
417 therefore could not explain the outgrowth delay. As for other spores, the enrichment of the  
418 growth medium by casamino acids (0.5%) increased the outgrowth rate of RM spores, which,  
419 nevertheless, remained below the WT level (Fig 7C). These results indicate that *rho* inactivation  
420 imposes stricter requirements on the spore outgrowth.

421 We asked whether Rho activity is needed exclusively during spore morphogenesis for the  
422 formation of an appropriate molecular basis for spore revival in the future, or for a correct  
423 metabolic resumption during spore outgrowth. To answer this question, we placed the *rho* gene  
424 under the control of the IPTG-inducible promoter P<sub>spac</sub>, which allowed us to selectively control  
425 *rho* expression during sporulation and/or spore outgrowth. By immunoblot analysis of P<sub>spac</sub>-  
426 *rho* cells using the Rho<sup>Bs</sup>-specific antiserum, we established that the induction of P<sub>spac</sub>-*rho* by  
427 IPTG (100μM) determines a near-natural level of Rho protein (Materials and Methods; S8 Fig).  
428 Following this, we allowed P<sub>spac</sub>-*rho* cells to sporulate in the presence or absence of IPTG  
429 100μM, purified the mature spores from the IPTG-induced and non-induced cultures and

430 compared the revival of two types of  $P_{\text{spac}}\text{-rho}$  spores in the conditions where *rho* expression  
431 was omitted or *de novo* induced by IPTG.

432 We observed that spores, which were formed in the absence of Rho ( $P_{\text{spac}}\text{-rho}^{(-\text{IPTG})}$ ), exhibited  
433 an accelerated germination like RM spores, while those that expressed *rho* during  
434 morphogenesis ( $P_{\text{spac}}\text{-rho}^{(+\text{IPTG})}$ ), germinated as WT (Fig 8A). Addition of IPTG together with  
435 the germinant did not modify germination kinetics of either spore type (Fig 8B). The two types  
436 of spores also behaved differently during outgrowth. In the absence of IPTG, the outgrowth of  
437  $P_{\text{spac}}\text{-rho}^{(-\text{IPTG})}$  spores was identical to RM spores, while  $P_{\text{spac}}\text{-rho}^{(+\text{IPTG})}$  spores grew out at an  
438 intermediate rate between WT and RM (Fig 8C). Interestingly, *de novo* induction of *rho*  
439 expression by IPTG had a small but reproducible stimulatory effect on the outgrowth rates, so  
440 that  $P_{\text{spac}}\text{-rho}^{(+\text{IPTG})}$  spores were able to “catch up” with the outgrowth of WT spores (Fig 8D).  
441 IPTG had no effect on the germination or outgrowth of WT and RM spores.

442 From these experiments, we conclude that normal spore revival requires expression of *rho*  
443 during spore morphogenesis and, although to a lesser extent, *de novo* during spore outgrowth.

444

445

## 446 **Discussion**

447

448 The main achievement of the present analysis is the revelation of spatiotemporal expression of  
449 the termination factor Rho during sporulation in *B. subtilis* via two distinct mechanisms: read-  
450 through transcription initiated at a distal promoter controlled by SigH in the mother cells, and  
451 transcription from the authentic SigF-dependent *rho* promoter in the forespores. These  
452 regulatory elements compensate for the inactivation of SigA-dependent *rho* expression at the  
453 end of exponential growth and allow the “refueling” of Rho protein in both compartments of  
454 the sporangium.

455 Our results also show that maintaining Rho levels during sporulation is necessary for the  
456 formation of spores with normal morphology, resistance properties and the ability to return to  
457 a vegetative state under favorable environmental conditions.

458

### 459 **Compartmentalized expression of *rho* during sporulation.**

460 The sporulation-specific read-through transcription of *rho* is initiated by the activation of the  
461 SigH-dependent promoter of *spo0F* gene encoding the phosphotransferase Spo0F of the Spo0A  
462 phosphorelay. The *spo0F* expression is regulated by Spo0A~P and constitutes one of the

463 positive feedback loops of Spo0A~P at the onset of sporulation (Lewandoski et al., 1986;  
464 Predich et al., 1992; Strauch et al., 1993; Asayama et al., 1995; Chastanet et al., 2010).  
465 Previously, we have established that Rho negatively regulates the expression of some  
466 components of the Spo0A phosphorelay, like the sensor kinase KinB (Bidnenko et al., 2017).  
467 Therefore, correct modulation of Spo0A~P activity at the initial steps of *B. subtilis*  
468 differentiation requires the decrease in the *rho* expression levels (Bidnenko et al., 2017). As we  
469 show here, this decrease is partially due to the silencing of the SigA-dependent *rho* promoter  
470 by yet unknown mechanism. It appears that alongside a self-reinforcing loop involving Spo0F,  
471 Spo0A~P simultaneously activates the Rho-mediated regulatory circuit, which can be viewed  
472 as a negative feedback loop of Spo0A~P. This regulatory function of Rho could be particularly  
473 important to fine-tune Spo0A~P activity during initiation of sporulation and in the mother cells,  
474 where Spo0A~P remains functional after asymmetric division (Fujita and Losick, 2003). Our  
475 data indicate that the mother cell-specific sigma factor SigE is not involved in the expression  
476 of *rho*. Nevertheless, inhibition of the *rho* read-through transcription results in the structural  
477 changes of spore coat, whose assembly depends on the activity of the SigE- and SigK-controlled  
478 genes (Eichenberger et al., 2003; Henriques and Moran, 2007; Driks and Eichenberger, 2016).  
479 This emphasizes an extended activity of Rho during the mother cell gene expression program.  
480 Identification of the alternative forespore-specific *rho* promoter matching the SigF-binding  
481 consensus allows us to classify *rho* as a member of the SigF regulon. Interestingly, an earlier  
482 analysis of forespore gene expression has detected the up-regulation of *rho* in sporulating *sigF*<sup>+</sup>  
483 *B. subtilis* cells (see Supplemental Table1 in Wang et al., 2006). However, *rho* was not induced  
484 by the artificial expression of SigF during exponential growth in LB, a second criterion used  
485 for gene classification to the SigF regulon (Wang et al., 2006). It is possible that, in that analysis,  
486 the untimely activated SigF failed to compete with the abundant vegetative SigA for binding to  
487 the overlapping cognate *rho* promoters. The silencing of the SigA-dependent *rho* promoter  
488 might facilitate SigF binding. However, the mechanism of this silencing is unclear, and despite  
489 some discrepancies between the reports, SigA remains active in the forespores (Lord et al.,  
490 1999; Fujita, 2000; Li et Piggot, 2001; Marquis et al., 2008; Riley et al., 2018; 2021). It is also  
491 notable that the *rho* gene is located within a chromosomal cluster of SigF-dependent genes  
492 activated the first during the forespore formation (Steil et al., 2005; Wang et al., 2006), what  
493 pinpoints its early expression. At the same time, our data indicate the role of Rho in the  
494 resistance of spores to ultraviolet radiation, the main factors of which, the  $\alpha/\beta$ -type small acid-  
495 soluble spore proteins (SASPs) and the spore photoproduct lyase SplB, are controlled by the  
496 late forespore-specific sigma factor SigG (Mason and Setlow, 1986; Pedraza-Reyes et al., 1994;

497 Setlow, 2001). Therefore, like the read-through transcription in the mother cells, the SigF-  
498 mediated *rho* expression appears to ensure Rho activity during the entire forespore-specific  
499 gene expression program. It can also mediate the packaging of Rho protein in mature spores,  
500 where it has been recurrently identified by mass spectrometric analysis (Swarge et al., 2020; Tu  
501 et al, 2020).

502

### 503 **Rho involvement in the spatiotemporal regulation of spore development.**

504 Two spore phenotypes, a decreased UV-resistance and a structurally altered outer coat, resulting  
505 from the complete inactivation of *rho*, or following the inhibition of *rho* expression in the  
506 forespores and in the mother cells, respectively, highlight the importance of the  
507 compartmentalized Rho-mediated transcription termination for spore development. Our  
508 previous transcriptome analysis of RM cells in stationary phase revealed disordered and  
509 untimely expression of many sporulation genes via their extensive sense or antisense read-  
510 through transcription or, more rarely, unscheduled activation of promoters (Bidnenko et al.,  
511 2023). The relevant gene expression changes are compiled in S1 Table and can be visualized at  
512 [http://genoscapist.migale.inrae.fr/seb\\_rho/](http://genoscapist.migale.inrae.fr/seb_rho/) (Bidnenko et al., 2023; Dérozier et al., 2021). We  
513 posit that at least some of the sporulation genes abnormally expressed in the stationary RM cells  
514 are subject to Rho-mediated regulation during sporulation. At the same time, we are aware that  
515 most of potential sporulation-specific targets of Rho are not yet expressed in stationary phase.  
516 For instance, the stationary phase transcriptome of RM cells does not provide an obvious  
517 explanation for the decreased UV-resistance of spores differentially expressing *rho*. Indeed, the  
518 observed upregulation of several *ssp* genes in the stationary RM cells, in particular *sspC*, is  
519 contrary to what one could expect if spores become sensitive to UV. It is therefore likely that  
520 the effect of Rho in stationary phase and in sporulating cells is different for some genes.

521 The existing transcriptome data probably provide the most straightforward mechanistic hints  
522 on the involvement of Rho in the regulation of spore coat morphogenesis. The prominent coat  
523 defects in RM and 3TER-mT/A spores resemble those induced by the inactivation of  
524 morphogenetic proteins CotO, CotH or CotG, or auxiliary proteins of coat assembly, superoxide  
525 dismutase SodA and holin YwcE (McPherson et al., 2005; Zilhão et al., 1999; Isticato et al.,  
526 2020; Freitas et al., 2020; Henriques et al., 1998; Real et al., 2005; Henriques and Moran, 2007).  
527 All of the abovementioned mutant spores exhibit a disordered, low electron-dense and thinner  
528 outer coat frequently detached from the inner layer. The protein kinase CotH and its target  
529 protein CotG were recently identified as the main morphogenetic factors determining the

530 regular structure of spore coat (Nguyen et al, 2016; Freitas et al., 2020; Isticato et al., 2020; Di  
531 Gregorio Barletta et al., 2022). It has been shown that phosphorylated CotG assembles in the  
532 coat, while its non-phosphorylated form sequesters other coat proteins in the mother cell  
533 cytoplasm (Di Gregorio Barletta et al., 2022).

534 Interestingly, the expression levels of *cotG* are strongly upregulated in RM cells, due to the  
535 transcription upshift at, or close to, the SigK-dependent *cotG* promoter and the read-through  
536 transcription initiated at the upstream *alsR* gene (Nicolas et al., 2012; Bidnenko et al., 2023; S1  
537 Table). The same read-through transcript appears antisense to the oppositely oriented  
538 neighboring genes *cotB* and *cotH*. We suggest that Rho participates in the control of the  
539 transcription of the *cotB-cotH-cotG* gene cluster during sporulation and that inactivation of the  
540 *rho* expression in the mother cells modifies the CotG-CotH protein balance important for  
541 correct assembly of CotG, thus leading to spore coat defects. Work is in progress to test this  
542 hypothesis.

543 Alongside the shared phenotypes linked to the inhibition of spatiotemporal expression of *rho*,  
544 RM spores are specifically characterized by the increased levels of DPA content. The synthesis  
545 of DPA and its transfer to the core across the spore membranes involves the protein products  
546 of both mother cell- and forespore-specific genes (Daniel and Errington, 1993; Ramírez-  
547 Guadiana et al., 2017b; Gao et al., 2022). None of the genes involved in the DPA metabolism  
548 are subject to unscheduled activation in RM cells in stationary phase. However, we detected  
549 strong induction of a defined SigA-dependent antisense promoter located within the SigG-  
550 regulated *spoVAA-spoVAB-spoVAC-spoVAD-spoVAEB-spoVAEA-spoVAF-lysA* operon,  
551 whose products are essential for DPA uptake into the core and release during germination  
552 (Tovar-Rojo et al., 2002; Gao et al., 2022; Nicolas et al., 2012; Bidnenko et al, 2023). In the  
553 wild type *B. subtilis* cells, this antisense promoter is weakly activated under some stress  
554 conditions and late in sporulation (Nicolas et al., 2012). Remarkably, in RM cells, the generated  
555 ~5 kb-long antisense transcript extends across *spoVAA*, *spoVAB*, *spoVAC* genes and the *dacF*-  
556 *spoIIAA-spoIIAB-sigF* operon. It remains to be established whether this antisense transcript  
557 affects the expression of the genes on the opposite strand during RM sporulation.

558

### 559 **Rho involvement in spore revival.**

560 RM spores also differ from their siblings by their impaired revival capacity, showing a rapid  
561 germination followed by slow outgrowth. The rate of germination in response to different  
562 nutrient stimuli is mainly determined by the levels of corresponding germinant receptors in the  
563 spore membrane (Cabrera-Martinez et al., 2003; Ghosh et al., 2012; Chen et al., 2014). The

564 RM stationary phase transcriptome showed unscheduled up-regulation of the SigG-controlled  
565 *gerBA-gerBB-gerBC* operon encoding the AGFK germinant receptor GerB (Corfe et al., 1994)  
566 and the SigK-controlled *gerPA-gerPB-gerPC-gerPD-gerPE-gerPF* operon, whose products  
567 facilitate the passage of nutrient germinants across the spore coat (Behravan et al., 2000).  
568 Although these features suggest that Rho controls both operons during sporulation, they seem  
569 insufficient to explain the rapid germination of RM spores in response to L-alanine or L-valine.  
570 Among the *gerAA-gerAB-gerAC* genes encoding the L-alanine germinant receptor GerA  
571 (Feavers et al, 1990; Amon et al., 2022, and references therein), only *gerAA* appears up-  
572 regulated ~3-fold in the stationary RM cells.

573 Interestingly, Rudner and colleagues identified *rho* among the genes, whose inactivation by  
574 Mariner transposon results in a premature germination of the developing spores triggered by  
575 the GerA receptor, probably in response to some undefined defects of spore envelope (Meeske  
576 et al., 2016; Ramírez-Guadiana et al., 2017). The authors report that GerA activity results in a  
577 decreased sporulation efficiency of the *rho::Mariner* mutant, which is opposite to our recurrent  
578 observation of a highly efficient sporulation in the *rho*-deleted RM cells. Nevertheless, the  
579 established genetic interaction between Rho and GerA proteins may be relevant to the  
580 germination phenotype of the mature RM spores, whose coat is severely altered. Moreover, the  
581 structure of RM spore coat suggests a lower level of coat protein cross-linking (Henriques and  
582 Moran, 2007), which can facilitate spore germination, as previously observed (Abhyankar et  
583 al., 2015). The germination rate of RM spores might be also influenced by high levels of DPA,  
584 a potent non-nutrient germinant that stimulates cortex hydrolysis by CwlJ hydrolase both  
585 directly and during nutrient-induced germination (Paidhungat and Setlow, 2000; Paidhungat et  
586 al., 2001).

587 More generally, spore germination is a complex highly heterogeneous process influenced by  
588 multiple factors, including, among others, the metabolic activity of cells during sporulation and  
589 the duration of spore formation (Segev et al. 2012; Bressuire-Isoard et al., 2018; Mutlu et al,  
590 2018, 2020; Riley et al., 2021; Rao et al., 2022). From this viewpoint, a more synchronous and  
591 rapid sporulation in RM population (Bidnenko et al., 2017, and this study) might result in a  
592 more homogeneous molecular composition of spores and, consequently, in a decreased  
593 heterogeneity of spore germination.

594 At the same time, the absence of Rho negatively affects the outgrowth of the germinated RM  
595 spores even in a nutrient-enriched medium. Therefore, *rho* inactivation imposes more stringent  
596 requirements for spore outgrowth, which in itself is more exacting than vegetative growth  
597 (O'Brien and Campbell, 1957). Taken together, a rapid germination and a slow outgrowth of

598 RM spores suggest that, in the wild type background, Rho determines the fitness of reviving  
599 spores.

600 Using a controlled *rho* expression system, we showed that the normal rate of spore outgrowth  
601 requires *rho* expression both during spore formation and after spore germination. During  
602 sporulation, Rho would ensure a proper composition of a spore molecular cargo required for  
603 spore revival, which also includes Rho protein itself (Mutlu et al, 2018; Rao et al., 2022; Swarge  
604 et al., 2020). After germination, Rho would be required in the ripening period, to control a  
605 proper termination of the actively resuming transcription, and later, during implementation of  
606 the transcription program of vegetative growth. This is consistent with the differential gene  
607 expression analysis of the reviving *B. subtilis* spores, which detected the upshifts in *rho*  
608 expression shortly after germination and at the end of outgrowth (Swarge et al., 2020). Most  
609 probably, the resumption of *rho* expression during outgrowth reflects the reactivation of SigA-  
610 dependent *rho* promoter.

611 To conclude, this and our previous analyses trace the activity of Rho through each stage of the  
612 complex program of *B. subtilis* sporulation, from the regulation of Spo0A~P activation at the  
613 onset of sporulation, through the subsequent morphogenesis of spores and up to the modulation  
614 of spore revival. This highlights the existence of specific targets for Rho-mediated transcription  
615 termination within the regulon of each alternative Sigma factor, which certainly include,  
616 alongside the known coding genes, a particular set of non-coding and anti-sense transcripts.  
617 Appropriate regulation of these targets requires in turn an accurate time- and spatial-specific  
618 regulation of the *rho* expression, through mechanisms we describe. Overall, our results  
619 strengthen our vision of Rho as a built-in regulatory module of *B. subtilis* cell differentiation.

620

621

## 622 **Materials and Methods**

623

### 624 **Bacterial strains and growth conditions**

625 All strains used in the analysis originate from *B. subtilis* 168 *trp*<sup>+</sup> strain BSB1 (Nicolas et al.,  
626 2012) and are listed in S2 Table. The *Escherichia coli* TG1 strain was used for construction of  
627 intermediate plasmids. Cells were routinely grown in liquid or solidified rich LB medium at  
628 37°C. Standard protocols were used for transformation of *E. coli* and *B. subtilis* competent cells  
629 (Harwood and Cutting, 1990). Sporulation of *B. subtilis* cells was induced by the method of  
630 nutrient exhaustion in supplemented Difco sporulation medium (DSM; Difco) (Schaeffer et al.,

631 1965) or by the resuspension method (Harwood and Cutting, 1990), as detailed in (Bidnenko et  
632 al., 2023). Optical density of the bacterial cultures was measured with NovaspecII Visible  
633 Spectrophotometer, Pharmacia Biotech. When required, antibiotics were added at following  
634 concentrations: 0.5  $\mu\text{g}$  per ml of erythromycin, 3  $\mu\text{g}$  per ml of phleomycin, 100  $\mu\text{g}$  per ml of  
635 spectinomycin, and 5  $\mu\text{g}$  per ml of chloramphenicol to *B. subtilis* cells; and 100  $\mu\text{g}$  per ml of  
636 ampicillin or 20  $\mu\text{g}$  per ml of kanamycin to the plasmid-containing *E. coli* cells. For the  
637 induction of  $P_{spac}$ -*rho* fusion, IPTG (isopropyl-  $\beta$ -D-1-thiogalactopyranoside) inducer was  
638 added to cells and spores to final concentration 100 $\mu\text{M}$ .

639

### 640 **Strains and plasmids construction**

641 All intermediate plasmids were constructed using Q5 High Fidelity DNA Polymerase and DNA  
642 modification enzymes purchased from New England Biolabs. Transcriptional fusion of the  
643 luciferase gene *luc* and the *rho* promoter ( $P_{rho}$ -*luc*) was constructed as follows. The  
644 oligonucleotide pairs glpXBam/veb738 were used to amplify a  $\sim$ 1 Kb fragment of *B. subtilis*  
645 chromosome located directly upstream the *rho* start codon. The 5' part of the *luc* gene was  
646 amplified from the plasmid pUC18cm-Luc (Mirouze et al., 2012) using oligonucleotides  
647 *lucintrev* and veb739 complementary to veb738. Two DNA fragments were joined by PCR  
648 using the primers glpXBam and *lucintrev*, and the resulting DNA fragment was cloned at  
649 pUC18cm-Luc using BamHI and BstBI endonucleases and T4 DNA ligase. The resulting  
650 plasmid pBRL862 was integrated by single crossover at the *rho* chromosomal locus of BSB1  
651 (WT) and BRL1 ( $\Delta$ *rho*) cells using selection for chloramphenicol-resistance. By this event, the  
652 *luc* gene was placed under all natural regulatory signals of the *rho* expression. In the WT  
653 background, the replaced intact copy of *rho* gene remained active under the control of own  
654 promoter.

655 Insertion of three intrinsic transcription terminators (3TER) upstream the chromosomal  $P_{rho}$ -*luc*  
656 fusion was performed as follows. The 3TER DNA fragment amplified from pMutin4 plasmid  
657 using oligonucleotides veb734 and veb735 was end-joined with the DNA fragments amplified  
658 from pBRL862 using the pairs of oligonucleotides glpXBam/veb798 (5'-complementary to  
659 veb734) and *lucintrev*/veb797 (5'-complementary to veb735). The primers glpXBam and  
660 *lucintrev* were used in the joining reaction. The PCR product was cut by EcoRV and BstBI  
661 endonucleases and cloned at a similarly cut and gel-purified pBRL862 plasmid. The resulting  
662 plasmid pBRL1107 was integrated at the *rho* locus of BSB1 chromosome as above. The created

663 3TER- $P_{rho}$ -*luc* transcriptional fusion contains intact 5'-UTR of *rho* and the 3TER insertion  
664 immediately after the *glpX* stop codon.

665 Transcriptional fusion between the *gfp* gene, encoding Green Fluorescent Protein, and the *rho*  
666 promoter ( $P_{rho}$ -*gfp*) was constructed similarly to  $P_{rho}$ -*luc*. The oligonucleotides *glpXBam* and  
667 *veb742* were used for amplification of the *rho* moiety from BSB1 chromosome, and the *gfp*  
668 gene was amplified from the plasmid pCVO119 using the primers *veb741* and *veb740*  
669 complementary to *veb742*. The primers *glpXBam* and *veb741* were used for joining PCR, and  
670 the resulting DNA fragment was cloned in pCVO119 plasmid using *BamHI* and *NcoI*  
671 endonucleases and T4 DNA ligase. The resulting plasmid pBRL893 was integrated by single  
672 crossover at the *rho* locus of the BSB1 chromosome using selection for spectinomycin  
673 resistance.

674 To construct the 3TER- $P_{rho}$ -*gfp* transcriptional fusion, the DNA fragment containing 3TER and  
675 the *rho* 5'-UTR was amplified from pBRL1107 plasmid using the primers *glpXBam* and  
676 *veb742* and fused to the *gfp* gene as described above for pBRL893. The product of joining PCR  
677 was cut by *EcoRV* and *NcoI* endonucleases and cloned at a similarly cut and gel-purified  
678 pBRL893. The resulting pBRL1150 plasmid was inserted in the BSB1 chromosome as above.  
679 Site-directed mutagenesis of the Sigma F-dependent *rho* promoter of the  $P_{rho}$ -*luc* and  $P_{rho}$ -*gfp*  
680 transcriptional fusions was performed as follows. The plasmids pBRL893 and pBRL1107 were  
681 entirely amplified using the pairs of side-by-side oligonucleotides *veb803/veb802*, containing  
682 a 5'-terminal C nucleotide to introduce the point mutation *mF-35T/C*, and *veb803/veb805*, with  
683 a 5'-terminal A for the point mutation *mF-35T/A*. The PCR products were phosphorylated using  
684 T4 polynucleotide kinase, self-ligated and treated with *DpnI* endonuclease to remove the  
685 template DNA prior transformation in *E. coli* cells. The resulting mutated derivatives of the  
686 plasmids pBRL893 (pBRL1141 and pBRL1164) and pBRL1107 (pBRL1116 and pBRL1162)  
687 were controlled by sequencing and inserted into the *B. subtilis* BSB1 chromosome as above to  
688 produce the mutated fusions *mF-35T/C P<sub>rho</sub>-gfp* and *mF-35T/A P<sub>rho</sub>-gfp* and 3TER *mF-35T/C*  
689  $P_{rho}$ -*luc* and 3TER *mF-35T/A P<sub>rho</sub>-luc*, respectively.

690 Structural modifications of the *rho* expression unit at natural locus were performed by the  
691 method for allelic replacement using a shuttle vector pMAD (Arnaud et al., 2004).

692 To insert 3TER transcription terminators at the *rho* locus, two DNA fragments amplified from  
693 the BSB1 chromosome with the pairs of oligonucleotides *veb795/veb796* and *veb797/veb798*  
694 were end-joined to the 3TER DNA fragment (see above) by PCR using the primers *veb795* and  
695 *veb796*. The product of joining PCR was cut with *BamHI* and *EcoRI* endonucleases and cloned  
696 in the pMAD vector (Arnaud et al., 2004). The resulting plasmid pBRL1108 was integrated

697 into the *rho* locus of the BSB1 chromosome with selection of the erythromycin-resistant  
698 transformants at 37°C non-permissive for plasmid replication. Single transformants were  
699 propagated in LB without antibiotic at 30°C to induce the loss of the vector and plated at LB-  
700 plates at 37°C. The erythromycin-sensitive clones were selected among the grown colonies and  
701 tested by PCR for the presence of the 3TER insertion using oligonucleotides veb734 and  
702 veb735, and the selected clones were controlled for structural integrity of the *glpX-3TER-rho*  
703 region by sequencing.

704 The point mutation *mF-35T/A* was introduced in the *rho* locus of BSB1 and BRL1130 (3TER)  
705 strains as follows. Two DNA fragments were amplified from pBRL1164 plasmid and BSB1  
706 chromosome by PCR with the respective pairs of oligonucleotides veb796/veb808 and  
707 veb806/veb807, complementary to veb808. The fragments were joined by PCR using veb796  
708 and veb806 as primers, and the resulting product was cloned at pMAD vector using BamHI and  
709 EcoRI endonucleases and T4 DNA ligase. The resulting plasmid was transformed into BSB1  
710 cells and the transformants were processed as described above to select the point mutant WT-  
711 mT/A. The mutant strain 3TER-mT/A was constructed in a similar way using the plasmid  
712 pBRL1162 as a template in the first PCR and WT-mT/A strain as a recipient for transformation.  
713 To construct the IPTG-controlled system for *rho* expression, the DNA fragment amplified from  
714 BSB1 chromosome by PCR with the oligonucleotides veb806 and veb880 was digested by  
715 EcoRI and BamHI endonucleases and clones at pMUTIN4 vector (Vagner et al., 1998). The  
716 resulting plasmid was transformed in BSB1 cells with selection to erythromycin resistance.  
717 For the purification of the *B. subtilis* Rho protein, *rho* gene was amplified by PCR with  
718 oligonucleotides veb596 and veb599, treated by NdeI and SalI endonucleases and cloned at the  
719 expression vector pET28a (Novagen) allowing expression of Rho with N-terminal hexa-  
720 histidine tag (Ingham et al., 1999). The resulting plasmid pETRho was transferred to *E. coli*  
721 strain BL21-CodonPlus (DE3)-RIL (Stratagene).

## 722 **Luciferase assay**

723 Analysis of promoters' activity using luciferase fusions was performed as described previously  
724 (Mirouze et al., 2011) with minor modifications detailed in (Bidnenko et al., 2023). Cells were  
725 grown in LB medium to mid-exponential phase (OD<sub>600</sub> 0,4-0,5), cultures were centrifuged and  
726 resuspended to OD 1.0 in fresh LB or DSM, to follow expression of the fusions during growth  
727 or sporulation, respectively. The pre-cultures were next diluted in respective media to OD<sub>600</sub>  
728 0.025. The starter cultures were distributed by 200µl in a 96-well black plate (Corning, USA)  
729 and Xenolight D-luciferin K-salt (Perkin, USA) was added to each well to a final concentration

730 of 1.5 mg/ml. The cultures were grown under strong agitation at 37°C and analyzed in Synergy  
731 2 Multi-mode microplate reader (BioTek Instruments). Relative Luminescence Units (RLU)  
732 and OD<sub>600</sub> were measured at 5 min intervals. Each fusion-containing strain was analyzed at  
733 least three times. Each experiment included four independent cultures of each strain.

734

### 735 **Epifluorescence microscopy and image processing**

736 For all microscopic observations, cells were mounted on a 2% agarose pad and topped with a  
737 coverslip. Bacteria were imaged with an inverted microscope (Nikon Ti-E) equipped with an  
738 iLas2 laser coupling system from Roper Scientific (150 mW, 488nm and 50 mW, 561 nm), a  
739 100× oil immersion phase objective, an ORCA-R2 camera (Hamamatsu) and controlled by the  
740 MetaMorph software package (v 7.8; Molecular Devices, LLC). The post-acquisition treatment  
741 of the images was done with the Fiji software (van Ooij et al., 2004; Schindelin et al., 2012).  
742 To determine the frequency of cells entering into sporulation, cultures were sampled three hours  
743 after the induction of sporulation by the resuspension method (Harwood and Cutting, 1990).  
744 Sampled cells were mixed with the lipophilic fluorescent dye Mitotracker Red (10 µg/ml final  
745 concentration) prior to microscopic observation. Asymmetric septa were manually counted in  
746 two independent replicas (N > 450 per strain and per replica).

747 To assess *rho* expression during sporulation using GFP as a reporter, cells bearing the non-  
748 modified or the point-mutated  $P_{rho}$ -*gfp* transcriptional fusions were induced for sporulation by  
749 the resuspension method and sampled as above. Sampled cells were mixed with the lipophilic  
750 fluorescent dyes Nile Red (10 µg/ml final concentration) prior to microscopic observation. To  
751 measure the fluorescence intensity in the different compartments, circular areas of a constant  
752 0.45 µm diameter were drawn in the center of individual compartments (forespores, mother  
753 cells, or predivisional cells) using images showing membrane-labelled cells, and recorded as a  
754 list of ROI. ROIs were subsequently applied over the corresponding image displaying the GFP  
755 signal, and the average fluorescence over each ROI recorded. Background fluorescence,  
756 determined as the average fluorescence from ROIs of identical areas spread over the field  
757 (outside cells), was subtracted to give the final fluorescence intensity of individual  
758 compartments. Counting was performed in at least two fields of view and for a minimum of  
759 800 cell compartments per strain, in two independent experiments. Plotted values are average  
760 fluorescence intensities from pooled replicas, thus standard deviations account for cell to cell  
761 variability across all fields and replicas.

762

### 763 **RNA preparation and Northern blotting**

764 Total RNA was extracted from *B. subtilis* cultures at OD<sub>600</sub> indicated in the text by the glass  
765 beads method (Bechhofer et al., 2008). For Northern blotting, 5 µg of RNA were separated on  
766 1% agarose-formaldehyde (2.2M) gel in MOPS (50mM)/EDTA (1mM) buffer (pH 7.0) and  
767 transferred to Hybond N+ membrane (GE-Healthcare) as described previously (Redko et al.,  
768 2013). Membrane pre-hybridization and the *rho* RNA detection by hybridization with the *rho*-  
769 specific  $\alpha^{32}\text{P}$ -labelled riboprobe was performed as detailed in (Gilet et al., 2020). The riboprobe  
770 was synthesized by T7 RNA polymerase in the presence of [ $\alpha$ -<sup>32</sup>P]UTP at the template of the  
771 purified PCR fragment obtained with oligonucleotides YRH1 and YRH2 (S3 Table). The  
772 reverse PCR primer YRH1 contained at the 5'-end the T7 RNA polymerase promoter sequence  
773 (TAATACGACTCACTATA).

774

### 775 **Sporulation assay**

776 Cells were induced for sporulation by the resuspension method, and the cultures were analyzed  
777 for the presence of spores starting from six hours after resuspension. The percentage of spores  
778 in a sample was calculated as proportion of viable cells after heating at 70°C for 15 min to the  
779 total number of cells as described in (Bidnenko et al., 2023).

780

### 781 **Spore purification and treatments**

782 *B. subtilis* cells growing exponentially in LB were suspended in DSM at OD<sub>600</sub> 0.05 and  
783 cultured at 37°C with aeration for 24 hours. Spores were purified by sequential rounds of  
784 intensive washing in ice-cold water and centrifugation over 3 days as described by Nicholson  
785 and Setlow in (Harwood and Cutting, 1990). The samples of the purified spores were controlled  
786 for the absence of cells by the heat-resistance test as described above and stored at 4°C in water  
787 at OD<sub>600</sub> > 10. The purity of standard spore samples was above 95 percent.

788 For electron microscopy analysis, spores were additionally purified on Nicodenz (Axis-Shield,  
789 United Kingdom) density gradients. Spores were suspended in 1 ml of 20 % Nicodenz solution,  
790 layered on 50 % Nicodenz (15 ml) in the centrifuge tubes and centrifuged at 14,000 x g for 30  
791 min at 10°C. The pelleted pure spores were washed 5 times in ice-cold water to remove traces  
792 of Nicodenz and kept at 4°C before analysis.

793 Prior the assays of spore resistance phenotypes and germination, the purified spores were  
794 suspended in 10 mM Tris HCl (pH 8.0) at OD<sub>600</sub> 1.0 and activated by heating at 70°C for 30  
795 min and subsequent cooling in ice for 20 min. The activated spores were used in the assays  
796 within 1 hour.

797 Chemical removal of spore coats was performed according to (Riesenman and Nicholson,  
798 2000). Spores were suspended in decoating solution (50 mM Tris base, 8 M urea, 50 mM  
799 dithiothreitol, 1% sodium dodecyl sulfate; pH 10.0) at OD<sub>600</sub> 5.0 and incubated at 60°C for 90  
800 min with vortexing. After the treatment, spores were intensively washed in STE buffer (150  
801 mM NaCl, 10 mM Tris-HCl, 1 mM EDTA; pH 8.0) as described.

802

### 803 **Transmission electron microscopy**

804 Purified spores were fixed with 2% glutaraldehyde in 0.1 M sodium cacodylate buffer (pH 7.2)  
805 for 1 h at room temperature. Samples were contrasted with 0.5% Oolong tea extract in  
806 cacodylate buffer and postfixed with 1% osmium tetroxide containing 1.5% potassium  
807 cyanoferrate. The samples were dehydrated and embedded in Epon (Delta Microscopies,  
808 France), as described (Theodorou et al., 2019). Thin sections (70 nm) were collected onto 200-  
809 mesh copper grids and counterstained with lead citrate. Grids were examined with a Hitachi  
810 HT7700 electron microscope operated at 80 kV, and images were acquired with a charge-  
811 coupled device camera (Advanced Microcopy Techniques; facilities were located on the  
812 MIMA2 platform [INRAE, Jouy-en-Josas, France;  
813 <https://doi.org/10.15454/1.5572348210007727E12>]). The post-acquisition treatment of the images  
814 and measurement of the thickness of the spore coat were performed using the Fiji software  
815 (Schindelin et al., 2012).

816

### 817 **Spore UV resistance assay**

818 The activated spores were suspended in Tris-HCl (pH 8.0) at OD<sub>600</sub> 0.5, pipetted in triplicates  
819 (50 µl) in the wells of 48-well sterile microtiter plates (Evergreen Scientific) and irradiated by  
820 ultraviolet (254 nm) light using Stratalinker 2400 UV Crosslinker (Stratagene) at the J/m<sup>2</sup> doses  
821 indicated in the text (one plate per UV dose). The irradiated spore suspensions were plated in  
822 sequential dilutions at LB plates and the colonies were counted after 24 hours of incubation at  
823 37 °C. The UV- resistance was determined as a ratio of the colony-forming units in the  
824 irradiated and non-irradiated samples of spores. Five experiments were performed with two  
825 independent sets of spores differentially expressing Rho.

826 To determine the effect of *rho* inactivation on the UV resistance of vegetative cells, WT and  
827 RM cultures in the late exponential phase (~10<sup>8</sup> cells/ml) were plated on LB plates and  
828 irradiated with the increasing doses of UV (254 nm) light using a Stratalinker 2400 UV

829 Crosslinker (Stratagene). The UV-resistance of cells was estimated as above. Three  
830 independent experiments were performed.

831

### 832 **Dipicolinic acid (DPA) assay**

833 The DPA content of spores was analyzed according to the protocol of Nicholson and Setlow  
834 (in Harwood and Cutting, 1990).

### 835 **Spore germination and outgrowth assay**

836 Spore germination and outgrowth assays were performed in MS medium (10.8 g l<sup>-1</sup> of K<sub>2</sub>HPO<sub>4</sub>,  
837 6 g l<sup>-1</sup> of KH<sub>2</sub>PO<sub>4</sub>, 1 g l<sup>-1</sup> of C<sub>6</sub>H<sub>5</sub>Na<sub>3</sub>O<sub>7</sub>·2H<sub>2</sub>O, 0.2 g l<sup>-1</sup> of MgSO<sub>4</sub>·7H<sub>2</sub>O, and 2 g l<sup>-1</sup> of K<sub>2</sub>SO<sub>4</sub>)  
838 supplemented with 0.5% glucose, 0.01% L-tryptophan, 0.1% glutamate, 0.1 mM of FeCl<sub>3</sub>  
839 citrate, 0.1 mM of CaCl<sub>2</sub>, 1 mM of MgSO<sub>4</sub> and trace elements (0.001 g l<sup>-1</sup> of MnCl<sub>2</sub> 4H<sub>2</sub>O,  
840 0.0017 g l<sup>-1</sup> of ZnCl<sub>2</sub>, 0.00043 g l<sup>-1</sup> of CuCl<sub>2</sub>· 2H<sub>2</sub>O, 0.0006 g l<sup>-1</sup> of CoCl<sub>2</sub> 6H<sub>2</sub>O and 0.0006 g  
841 l<sup>-1</sup> of Na<sub>2</sub>MoO<sub>4</sub>· 2H<sub>2</sub>O). The stock solutions (100mM) of L-alanine and L-valine germinants  
842 were prepared in 10 mM Tris-HCl buffer (pH 8.0) containing 10mM D-glucose and 100mM  
843 KCl. The stock solution of AGFK germinant mixture contained 100 mM L-asparagine, 10mM  
844 D-glucose, 10 mM D-fructose and 100mM KCl in 10 mM Tris-HCl buffer (pH 8.0). The  
845 activated spores were diluted to OD<sub>600</sub> 0.2 in the cold MS medium and distributed by 135 µl in  
846 the 96-well plate. Spore suspensions were simultaneously induced for germination by adding  
847 15µl of a stock germinant solution, incubated under strong agitation at 37°C and monitored for  
848 OD<sub>600</sub> at 2 min intervals in Synergy 2 Multi-mode microplate reader (BioTek Instruments). It  
849 usually took ~1 min between germinant addition and the first OD<sub>600</sub> reading. When needed, the  
850 stock solution of the germinant L-alanine was supplemented with 1mM IPTG or 5% casamino  
851 acids to get their final concentrations in spore suspensions 100µM and 0.5%, respectively.  
852 Three independently prepared sets of spores were used in the analysis. The assays were  
853 performed with each set of spores at least twice and included up to six replicas of each spore  
854 suspension in the same plate.

### 855 **Purification of the *B. subtilis* Rho protein for antibody preparation**

856 *E. coli* BL21-CodonPlus (DE3)-RIL cells containing pETRho were grown to an OD<sub>600</sub> of 0.2  
857 in a 400 ml culture (2YT medium) at 16°C, and Rho expression was induced by the addition of  
858 0.5 mM IPTG with continued growth overnight. The culture was harvested, pelleted and frozen  
859 at -80°C until further use. The frozen cells were resuspended in 10 ml of lysis buffer at 4°C  
860 containing 20 mM Tris-HCl pH 9.0, 100 mM Na<sub>2</sub>HPO<sub>4</sub>, 0.3 M NaCl, 10% glycerol and 0.1%

861 Triton X-100, to which were added 10 mg/ml DNase I and an EDTA-free anti-protease tablet  
862 (Roche). The suspension was passed twice through a French press (20 000 p.s.i.) and the lysate  
863 centrifuged for 30 min at 15 000 g. Imidazole-HCl (pH 8.0) was added to the supernatant to  
864 give a final concentration of 1 mM and the resultant suspension was applied to a 1 ml Ni<sup>2+</sup>-  
865 NTA column (Qiagen). The resin was then washed sequentially with 10 ml of lysis buffer  
866 (without Triton X-100), 10 ml of buffer containing 20 mM Tris-HCl pH 9.0, 0.3 M NaCl,  
867 20 mM Imidazole and, finally, 10 ml 20 mM Tris-HCl pH 9.0, 0.3 M NaCl and 250 mM  
868 Imidazole. *B. subtilis* Rho was eluted with 20 mM Tris-HCl pH 9.0, 100 mM Na<sub>2</sub>HPO<sub>4</sub>, 0.3 M  
869 NaCl and 500 mM Imidazole as 1ml fractions into collection tubes pre-filled with 3 ml elution  
870 buffer lacking Imidazole, to immediately dilute the sample 4-fold and avoid precipitation. The  
871 protein peak was determined initially by measuring the protein concentration (Bio-Rad) in the  
872 different fractions. Peak fractions were pooled and dialyzed over-night in buffer containing  
873 20 mM Tris-HCl pH 9.0, 100 mM Na<sub>2</sub>HPO<sub>4</sub>, 0.3 M NaCl, 10% glycerol. Protein purity was  
874 verified by SDS-PAGE analysis and estimated at >95%. A sample of purified *B. subtilis* Rho  
875 protein at 1.1 mg/ml in storage buffer was filtered through 5µm, 0.5µm and then 0.2µm  
876 Acrodisc filters before rabbit immunization to generate custom anti-Rho polyclonal antibodies  
877 through the commercial '87-day anti-antigen classical' program of Eurogentec (Belgium). The  
878 low solubility of *B. subtilis* Rho in buffers suitable for immobilization on affinity  
879 chromatography columns prevented further purification of the anti-Rho antibodies from the  
880 crude sera. The best anti-Rho serum aliquot was selected from the immunization program  
881 aliquots by Western blotting with purified *B. subtilis* Rho and *B. subtilis* cell extract samples.

882

### 883 **Western blotting**

884 The crude cell extracts were prepared using Vibracell 72408 sonicator (Bioblock scientific).  
885 Bradford assay was used to determine total protein concentration in each extract. Equal amounts  
886 of total proteins were separated by SDS-PAGE (10% polyacrylamide). After the run, proteins  
887 were transferred to Hybond PVDF membrane (GE Healthcare Amersham, Germany), and the  
888 transfer quality was evaluated by staining the membrane with Ponceau S (Sigma-Aldrich). The  
889 Rho protein was visualized by hybridization with antiserum against *B. subtilis* Rho (Eurogentec,  
890 Belgium; dilution 1:5,000) and the secondary peroxidase-coupled anti-rabbit IgG antibodies  
891 A0545 (Sigma-Aldrich; dilution 1:20,000).

892

893

## 894 **References**

895

896 1. Peters JM, Vangeloff AD, Landick R. Bacterial transcription terminators: the RNA 3'-  
897 end chronicles. *J Mol Biol.* 2011; 412: 793-813.

898 2. Ray-Soni A, Bellecourt MJ, Landick R. Mechanisms of bacterial transcription  
899 termination: all good things must end. *Annu Rev Biochem.* 2016; 85: 319-347.

900 3. Kriner MA, Sevostyanova A, Groisman EA. Learning from the leaders: gene regulation  
901 by the transcription termination factor Rho. *Trends Biochem Sciences.* 2016; 41: 690-  
902 699.

903 4. Turnbough Jr CL. Regulation of bacterial gene expression by transcription attenuation.  
904 *Microbiol Mol Biol Rev.* 2019; 83: 10-1128.

905 5. Mandell ZF, Zemba D, Babitzke P. Factor-stimulated intrinsic termination: getting by  
906 with a little help from some friends. *Transcription.* 2022a; 1-13.

907 6. Roberts JW. Termination factor for RNA synthesis. *Nature.* 1969; 224: 1168-1174.

908 7. Quirk PG, Dunkley Jr EA, Lee P, & Krulwich TA. Identification of a putative *Bacillus*  
909 *subtilis* rho gene. *J Bacteriol.* 1993; 175: 647-654.

910 8. Peters JM, Mooney RA, Kuan PF, Rowland JL, Keles S, and Landick R. Rho directs  
911 widespread termination of intragenic and stable RNA transcription. *Proc Natl Acad Sci*  
912 *USA.* 2009; 106: 15406–15411.

913 9. Hao Z, Svetlov V & Nudler E. Rho-dependent transcription termination: A revisionist  
914 view. *Transcription.* 2021; 12: 171-181.

915 10. Mandell ZF, Vishwakarma RK, Yakhnin H, Murakami KS, Kashlev M, & Babitzke P.  
916 Comprehensive transcription terminator atlas for *Bacillus subtilis*. *Nature Microbiol.*  
917 2022b; 7: 1918-1931.

918 11. Song E, Uhm H, Munasingha PR, Hwang S, Seo YS ... & Hohng S. Rho-dependent  
919 transcription termination proceeds via three routes. *Nature Commun.* 2022; 13: 1-12.

920 12. Molodtsov V, Wang C, Firlar E, Kaelber JT, & Ebright RH. Structural basis of Rho-  
921 dependent transcription termination. *Nature.* 2023; 614: 367-374.

922 13. Murayama Y, Ehara H, Aoki M, Goto M, Yokoyama T, & Sekine SI. Structural basis  
923 of the transcription termination factor Rho engagement with transcribing RNA  
924 polymerase from *Thermus thermophilus*. *Science Advances.* 2023; 9: eade7093.

925 14. Rashid F, & Berger J. Protein structure terminates doubt about how transcription stops.  
926 *Nature.* 2023; 614: 237-238.

- 927 15. Nicolas P, Mäder U, Dervyn E, Rochat T, Leduc A, ... & Noirot P. Condition-dependent  
928 transcriptome reveals high-level regulatory architecture in *Bacillus subtilis*. *Science*.  
929 2012; 335: 1103-1106.
- 930 16. Peters JM, Mooney RA, Grass JA, Jessen ED, Tran F, Landick R. Rho and NusG  
931 suppress pervasive antisense transcription in *Escherichia coli*. *Genes Dev*. 2012;  
932 26:2621–2633
- 933 17. Mäder U, Nicolas P, Depke M, Pané-Farré J, Debarbouille M, ... & van Dijl JM.  
934 *Staphylococcus aureus* Transcriptome Architecture: From Laboratory to Infection-  
935 Mimicking Conditions. *PLoS Genet*. 2016; 1: e1005962.
- 936 18. Botella L, Vaubourgeix J, Livny J, & Schnappinger D. Depleting *Mycobacterium*  
937 tuberculosis of the transcription termination factor Rho causes pervasive transcription  
938 and rapid death. *Nature Commun*. 2017; 8:1-10.
- 939 19. Bidnenko V, Nicolas P, Grylak-Mielnicka A, Delumeau O, ... & Bidnenko, E.  
940 Termination factor Rho: from the control of pervasive transcription to cell fate  
941 determination in *Bacillus subtilis*. *PLoS Genet*. 2017; 13: e1006909.
- 942 20. Bidnenko V, Nicolas P, Guérin C, Dérozier S, Chastanet A, Dairou J, ... & Bidnenko E.  
943 Termination factor Rho mediates transcriptional reprogramming of *Bacillus subtilis*  
944 stationary phase. *PLoS Genet*. 2023; 19: e1010618.
- 945 21. Nagel A, Michalik S, Debarbouille M, Hertlein T, Gesell Salazar M, ... & Mäder U.  
946 Inhibition of rho activity increases expression of SaeRS-dependent virulence factor  
947 genes in *Staphylococcus aureus*, showing a link between transcription termination,  
948 antibiotic action, and virulence. *MBio*. 2018; 9: e01332-18.
- 949 22. Trzilova D, Anjuwon-Foster BR, Torres Rivera D, & Tamayo R. Rho factor mediates  
950 flagellum and toxin phase variation and impacts virulence in *Clostridioides difficile*.  
951 *PLoS Pathog*. 2020; 16: e1008708.
- 952 23. Lin Y, Alstrup M, Pang JKY, Maróti G, Er-Rafik M, Tourasse N, ... & Kovács ÁT.  
953 Adaptation of *Bacillus thuringiensis* to Plant Colonization Affects Differentiation and  
954 Toxicity. *Msystems*. 2021; 6: e00864-21.
- 955 24. Kryptou E, Townsend GE, Gao X, Tachiyama S, Liu , Pokorzynski N. D., ... &  
956 Groisman EA. Bacteria require phase separation for fitness in the mammalian gut.  
957 *Science*. 2023; 379: 1149-1156.
- 958 25. Lee YH, & Helmann JD. Mutations in the primary sigma factor  $\sigma_a$  and termination  
959 factor rho that reduce susceptibility to cell wall antibiotics. *J Bacteriol*. 2014; 196: 3700-  
960 3711.

- 961 26. Liu B, Kearns DB, Bechhofer DH. Expression of multiple *Bacillus subtilis* genes is  
962 controlled by decay of *slrA* mRNA from Rho dependent 3' ends. *Nucleic Acids Res.*  
963 2016; 44:3364–3372.
- 964 27. Hafeezunnisa M, & Sen R. The Rho-dependent transcription termination is involved in  
965 broad-spectrum antibiotic susceptibility in *Escherichia coli*. *Front Microbiol.* 2020; 11:  
966 3059.
- 967 28. Figueroa-Bossi N, Sánchez-Romero MA, Kerboriou P, Naquin D, ... & Bossi L.  
968 Pervasive transcription enhances the accessibility of H-NS–silenced promoters and  
969 generates bistability in *Salmonella* virulence gene expression. *Proc Natl Acad Sci USA.*  
970 2022; 119: e2203011119.
- 971 29. de Hoon MJ, Eichenberger P, Vitkup D. Hierarchical evolution of the bacterial  
972 sporulation network. *Curr Biol.* 2010; 20: R735–R745.
- 973 30. Swick MC, Koehler TM, Driks A. Surviving Between Hosts: Sporulation and  
974 Transmission. *Microbiol Spectr.* 2016; 4:10.
- 975 31. Galperin MY, Yutin N, Wolf YI, Vera Alvarez R, Koonin EV. Conservation and  
976 Evolution of the Sporulation Gene Set in Diverse Members of the Firmicutes. *J*  
977 *Bacteriol.* 2022; 21: e0007922.
- 978 32. Setlow P. Spore germination. *Curr Opin Microbiol.* 2003; 6: 550-556.
- 979 33. Setlow P, Wang S, & Li YQ. Germination of spores of the orders Bacillales and  
980 Clostridiales. *Annual Rev Microbiol.* 2017; 71: 459-477.
- 981 34. Setlow P, & Christie G. New Thoughts on an Old Topic: Secrets of Bacterial Spore  
982 Resistance Slowly Being Revealed. *Microbiol Mol Biol Rev.* 2023; e00080-22.
- 983 35. Segev E, Rosenberg A, Mamou G, Sinai L, & Ben-Yehuda S. Molecular kinetics of  
984 reviving bacterial spores. *J Bacteriol.* 2013; 195: 1875-1882.
- 985 36. Abhyankar WR, Kamphorst K, Swarge BN, Van Veen H,... & De Koning LJ. The  
986 influence of sporulation conditions on the spore coat protein composition of *Bacillus*  
987 *subtilis* spores. *Frontiers Microbiol.* 2016; 7: 1636.
- 988 37. Boone T, & Driks A. Protein synthesis during germination: shedding new light on a  
989 classical question. *J Bacteriol.* 2016; 198: 3251-3253.
- 990 38. Mutlu A, Trauth S, Ziesack M, Nagler K, ... & Bischofs IB. Phenotypic memory in  
991 *Bacillus subtilis* links dormancy entry and exit by a spore quantity-quality tradeoff. *Nat*  
992 *Commun.* 2018; 9: 69.

- 993 39. Mutlu, A., Kaspar, C., Becker, N., & Bischofs, I. B. A spore quality–quantity tradeoff  
994 favors diverse sporulation strategies in *Bacillus subtilis*. *The ISME J.* 2020; 14: 2703-  
995 2714.
- 996 40. Errington J. *Bacillus subtilis* sporulation: regulation of gene expression and control of  
997 morphogenesis. *Microbiol Rev.* 1993; 57:1-33.
- 998 41. Stragier P, Losick R. Molecular genetics of sporulation in *Bacillus subtilis*. *Annu Rev*  
999 *Genet.* 1996; 30:297-41.
- 1000 42. Piggot PJ, Hilbert DW. Sporulation of *Bacillus subtilis*. *Curr Opin Microbiol.* 2004; 7:  
1001 579-86.
- 1002 43. Higgins, D., Dworkin, J. Recent progress in *Bacillus subtilis* sporulation, *FEMS*  
1003 *Microbiol Rev.* 2012; 36: 131–148.
- 1004 44. Eichenberger P, Jensen ST, Conlon EM, van Ooij C, ... & Losick R. The  $\sigma^E$  regulon  
1005 and the identification of additional sporulation genes in *Bacillus subtilis*. *J Mol Biol.*  
1006 2003; 327: 945–972.
- 1007 45. Eichenberger P, Fujita M, Jensen ST, Conlon EM, ... & Losick R. The program of gene  
1008 transcription for a single differentiating cell type during sporulation in *Bacillus subtilis*.  
1009 *PLoS Biol.* 2004; 2:e328.
- 1010 46. Steil L, Serrano M, Henriques AO, Völker U. Genome-wide analysis of temporally  
1011 regulated and compartment-specific gene expression in sporulating cells of *Bacillus*  
1012 *subtilis*. *Microbiol.* 2005; 151: 399-420.
- 1013 47. Wang ST, Setlow B, Conlon EM, Lyon JL, Imamura D, Sato T, Setlow P, Losick R,  
1014 Eichenberger P. The forespore line of gene expression in *Bacillus subtilis*. *J Mol Biol.*  
1015 2006; 21: 16-37.
- 1016 48. de Hoon MJ, Eichenberger P, Vitkup D. Hierarchical evolution of the bacterial  
1017 sporulation network. *Curr Biol.* 2010; 20: R735–R745.
- 1018 49. Overkamp W, Kuipers OP. Transcriptional Profile of *Bacillus subtilis* sigF-Mutant  
1019 during Vegetative Growth. *PLoS One.* 2015; 27: e0141553.
- 1020 50. Meeske AJ, Rodrigues CD, Brady J, Lim HC, Bernhardt TG, Rudner DZ. High-  
1021 Throughput Genetic Screens Identify a Large and Diverse Collection of New  
1022 Sporulation Genes in *Bacillus subtilis*. *PLoS Biol.* 2016; 14: e1002341.
- 1023 51. Ingham CJ, Dennis J, Furneaux PA. Autogenous regulation of transcription  
1024 termination factor Rho and the requirement for Nus factors in *Bacillus subtilis*. *Mol*  
1025 *Microbiol.* 1999; 31: 651-663.

- 1026 52. Barik S, Bhattacharya P, & Das A. Autogenous regulation of transcription termination  
1027 factor Rho. *J Mol Biol.* 1985; 182: 495-508.
- 1028 53. Matsumoto Y, Shigesada K, Hirano M, Imai M. Autogenous regulation of the gene for  
1029 transcription termination factor rho in *Escherichia coli*: Localization and function of its  
1030 attenuators. *J Bacteriol.* 1986; 166: 945–958.
- 1031 54. Italiani VC, & Marques MV. The transcription termination factor Rho is essential and  
1032 autoregulated in *Caulobacter crescentus*. *J Bacteriol.* 2005; 187: 4290-4294.
- 1033 55. Silva IJ, Barahona S, Eyraud A, Lalaouna D, Figueroa-Bossi N, ... & Arraiano CM.  
1034 SraL sRNA interaction regulates the terminator by preventing premature transcription  
1035 termination of rho mRNA. *Proc Natl Acad Sci USA.* 2019; 116: 3042-3051.
- 1036 56. Mirouze N, Desai Y, Raj A, Dubnau D. Spo0A~P imposes a temporal gate for the  
1037 bimodal expression of competence in *Bacillus subtilis*. *PLoS Genet.* 2012; 8:  
1038 e1002586.
- 1039 57. Lewandoski M, Dubnau E, Smith I. Transcriptional Regulation of the spo0F Gene of  
1040 *Bacillus subtilis*. *J Bacteriol* 1986; 168: 870-877
- 1041 58. Predich M, Nair G, Smith I. *Bacillus subtilis* early sporulation genes kinA, spo0F, and  
1042 spo0A are transcribed by the RNA polymerase containing sigma H. *J Bacteriol.* 1992;  
1043 174: 2771–2778.
- 1044 59. Strauch MA, Wu J-J, Jonas RH and Hoch JA. A positive feedback loop controls  
1045 transcription of the spo0F gene, a component of the sporulation phosphorelay In  
1046 *Bacillus subtilis*. *Molecular Microbiology.* 1993; 7: 967-974.
- 1047 60. Asayama M, Yamamoto A. & Kobayashi Y. Dimer form of phosphorylated Spo0A, a  
1048 transcriptional regulator, stimulates the spo0F transcription at the initiation of  
1049 sporulation in *Bacillus subtilis*. *J Mol Biol.* 1995; 250, 11–23.
- 1050 61. Vagner V, Dervyn E, & Ehrlich SD. A vector for systematic gene inactivation in  
1051 *Bacillus subtilis*. *Microbiology.* 1998; 144: 3097-3104.
- 1052 62. Illing N. & Errington J. Genetic regulation of morphogenesis in *Bacillus subtilis*: roles  
1053 of sigma E and sigma F in prespore engulfment. *J Bacteriol.* 1991; 173: 3159–3169.
- 1054 63. Setlow B, Magill N, Febroriello P, Nakhimovsky L, Koppel DE, and Setlow P.  
1055 Condensation of the forespore nucleoid early in sporulation of *Bacillus* species. *J*  
1056 *Bacteriol.* 1991; 173: 6270–6278.
- 1057 64. Lewis PJ, Partridge SR, Errington J. Sigma factors, asymmetry, and the determination  
1058 of cell fate in *Bacillus subtilis*. *Proc Natl Acad Sci USA.* 1994; 91: 3849–3853

- 1059 65. Eichenberger P, Fawcett P, Losick R. A three-protein inhibitor of polar septation during  
1060 sporulation in *Bacillus subtilis*. *Mol Microbiol.* 2001; 42: 1147–1162
- 1061 66. Londono-Vallejo JA, & Stragier P. Cell-cell signaling pathway activating a  
1062 developmental transcription factor in *Bacillus subtilis*. *Genes & development.* 1995; 9:  
1063 503-508.
- 1064 67. Wang ST, Setlow B, Conlon EM, Lyon JL, Imamura D, ... & Eichenberger P. The  
1065 forespore line of gene expression in *Bacillus subtilis*. *J Mol Biol.* 2006; 358: 16-37.
- 1066 68. Amaya E, Khvorova A, & Piggot PJ. Analysis of Promoter Recognition In Vivo  
1067 Directed by  $\zeta$ F of *Bacillus subtilis* by Using Random-Sequence Oligonucleotides. *J*  
1068 *Bacteriol.* 2001; 183: 3623-3630.
- 1069 69. Setlow P. Spores of *Bacillus subtilis*: their resistance to and killing by radiation, heat  
1070 and chemicals, *Journal of Applied Microbiology.* 2006; 101: 514–525.
- 1071 70. Henriques AO, & Moran Jr, CP. Structure, assembly, and function of the spore surface  
1072 layers. *Annu Rev. Microbiol.* 2007; 61: 555-588.
- 1073 71. Nicholson WL, Munakata N, Horneck G, Melosh HJ, Setlow P. Resistance of *Bacillus*  
1074 endospores to extreme terrestrial and extraterrestrial environments. *Microbiol Mol Biol*  
1075 *Rev.* 2000; 64: 548-72.
- 1076 72. Setlow P. Spore resistance properties. *The bacterial spore: from molecules to systems.*  
1077 *Microbiol Spectr.* 2016; 2: 201-215.
- 1078 73. Mason JM, Setlow P. Essential role of small, acid-soluble spore proteins in resistance  
1079 of *Bacillus subtilis* spores to UV light. *J Bacteriol.* 1986; 167:174-178.
- 1080 74. Pedraza-Reyes M, Gutiérrez-Corona F, Nicholson WL. Temporal regulation and  
1081 forespore-specific expression of the spore photoproduct lyase gene by sigma-G RNA  
1082 polymerase during *Bacillus subtilis* sporulation. *J Bacteriol.* 1994; 176: 3983-91.
- 1083 75. Setlow P. I will survive: DNA protection in bacterial spores. *Trends in Microbiology,*  
1084 2007; 15: 172-180.
- 1085 76. McKenney PT, Driks A, & Eichenberger P. The *Bacillus subtilis* endospore: assembly  
1086 and functions of the multilayered coat. *Nature Rev Microbiol.* 2013; 11: 33-44.
- 1087 77. Driks A, Eichenberger P. The Spore Coat. *The bacterial spore: from molecules to*  
1088 *systems. Microbiol Spectr.* 2016; 4.
- 1089 78. Setlow, P. Summer meeting 2013–when the sleepers wake: the germination of spores  
1090 of *Bacillus* species. *J Appl Microbiol.* 2013; 115: 1251-1268.

- 1091 79. Sinai L, Rosenberg A, Smith Y, Segev E, & Ben-Yehuda S. The molecular timeline of  
1092 a reviving bacterial spore. *Mol Cell*. 2015 57: 695-707.
- 1093 80. Ramírez-Guadiana FH, Meeske AJ, Wang X, Rodrigues CDA, Rudner DZ. The *Bacillus*  
1094 *subtilis* germinant receptor GerA triggers premature germination in response to  
1095 morphological defects during sporulation. *Mol Microbiol*. 2017a; 105: 689-704.
- 1096 81. Christie G, & Setlow P. *Bacillus* spore germination: Knowns, unknowns and what we  
1097 need to learn. *Cellular Signalling*. 2020; 74: 109729.
- 1098 82. Rosenberg A, Soufi B, Ravikumar V, Soares NC, Krug K, Smith Y, ... & Ben-Yehuda  
1099 S. Phosphoproteome dynamics mediate revival of bacterial spores. *BMC biology*, 2015;  
1100 13: 1-19.
- 1101 83. Chastanet A, Vitkup D, Yuan GC, Norman TM, Liu JS, Losick RM. Broadly  
1102 heterogeneous activation of the master regulator for sporulation in *Bacillus subtilis*.  
1103 *Proc Natl Acad Sci USA*. 2010; 107: 8486–8491.
- 1104 84. Fujita M & Losick R. The master regulator for entry into sporulation in *Bacillus subtilis*  
1105 becomes a cell-specific transcription factor after asymmetric division. *Genes & Dev*.  
1106 2003; 17: 1166-1174.
- 1107 85. Lord M, Barilla D, & Yudkin MD. Replacement of vegetative  $\zeta A$  by sporulation-  
1108 specific  $\zeta F$  as a component of the RNA polymerase holoenzyme in sporulating *Bacillus*  
1109 *subtilis*. *J Bacteriol*. 1999; 181: 2346-2350.
- 1110 86. Fujita M. Temporal and selective association of multiple sigma factors with RNA  
1111 polymerase during sporulation in *Bacillus subtilis*. *Genes to Cells*. 2000; 5: 79-88.
- 1112 87. Li Z. & Piggot PJ. Development of a two-part transcription probe to determine the  
1113 completeness of temporal and spatial compartmentalization of gene expression during  
1114 bacterial development. *Proc Natl Acad Sci USA*. 2001; 98: 12538-12543.
- 1115 88. Marquis KA, Burton BM, Nollmann M, Ptacin JL, Bustamante C, Ben-Yehuda, S, &  
1116 Rudner DZ. SpoIIIE strips proteins off the DNA during chromosome translocation.  
1117 *Genes & Dev*. 2008; 22:1786-1795.
- 1118 89. Riley EP, Trinquier A, Reilly ML, Durchon M, Perera VR, Pogliano K, & Lopez-  
1119 Garrido J. Spatiotemporally regulated proteolysis to dissect the role of vegetative  
1120 proteins during *Bacillus subtilis* sporulation: cell-specific requirement of  $\sigma H$  and  $\sigma A$ .  
1121 *Mol Microbiol*. 2018; 108: 45-62.

- 1122 90. Riley EP, Lopez-Garrido J, Sugie J, Liu RB, & Pogliano K. Metabolic differentiation  
1123 and intercellular nurturing underpin bacterial endospore formation. *Sci Adv.* 2021; 7:  
1124 eabd6385.
- 1125 91. Setlow, P. Resistance of spores of *Bacillus* species to ultraviolet light. *Environ Mol*  
1126 *Mutagenesis.* 2001; 38: 97-104.
- 1127 92. Swarge B, Abhyankar W, Jonker M, Hoefsloot H, Kramer G, Setlow P, Brul S, de  
1128 Koning LJ. Integrative Analysis of Proteome and Transcriptome Dynamics during  
1129 *Bacillus subtilis* Spore Revival. *mSphere.* 2020; 5:e00463-20.
- 1130 93. Tu Z, Dekker HL, Roseboom W, Swarge BN, Setlow P, Brul S, Kramer G. High  
1131 Resolution Analysis of Proteome Dynamics during *Bacillus subtilis* Sporulation.  
1132 *International Journal of Molecular Sciences.* 2021; 22: 9345.
- 1133 94. Dérozier S, Nicolas P, Mäder U, & Guérin C. Genoscapist: online exploration of  
1134 quantitative profiles along genomes via interactively customized graphical  
1135 representations. *Bioinformatics.* 2021; 37: 2747-2749.
- 1136 95. McPherson DC, Kim H, Hahn M, Wang R, Grabowski P, Eichenberger P, Driks A.  
1137 Characterization of the *Bacillus subtilis* spore morphogenetic coat protein CotO. *J*  
1138 *Bacteriol.* 2005; 187: 8278-90.
- 1139 96. Zilhão R, Naclerio G, Henriques AO, Baccigalupi L, Moran CP Jr, Ricca E. Assembly  
1140 requirements and role of CotH during spore coat formation in *Bacillus subtilis*. *J*  
1141 *Bacteriol.* 1999; 181: 2631-3.
- 1142 97. Isticato R., Lanzilli, M., Petrillo, C., Donadio, G., Baccigalupi, L., & Ricca, E. *Bacillus*  
1143 *subtilis* builds structurally and functionally different spores in response to the  
1144 temperature of growth. *Environ Microbiol.* 2020; 22: 170-182.
- 1145 98. Freitas C, Plannic J, Isticato R, ... & Henriques AO. A protein phosphorylation module  
1146 patterns the *Bacillus subtilis* spore outer coat. *Mol Microbiol.* 2020; 114: 934– 951.
- 1147 99. Henriques AO, Melsen LR, Moran CP Jr. Involvement of superoxide dismutase in spore  
1148 coat assembly in *Bacillus subtilis*. *J Bacteriol.* 1998; 180: 2285-91.
- 1149 100. Real G, Pinto SM, Schyns G, Costa T, Henriques AO, Moran CP Jr. A gene  
1150 encoding a holin-like protein involved in spore morphogenesis and spore germination  
1151 in *Bacillus subtilis*. *J Bacteriol.* 2005; 187:6443-53.
- 1152 101. Nguyen KB, Sreelatha A, Durrant ES, Lopez-Garrido J, Muszewska A,  
1153 Dudkiewicz M, ... & Tagliabracci VS. Phosphorylation of spore coat proteins by a  
1154 family of atypical protein kinases. *Proc Natl Acad Sci USA.* 2016; 113: E3482-E3491

- 1155 102. Isticato R, Lanzilli M, Petrillo C, Donadio G, Baccigalupi L, & Ricca E. *Bacillus*  
1156 *subtilis* builds structurally and functionally different spores in response to the  
1157 temperature of growth. *Environ Microbiol.* 2020; 22: 170-182.
- 1158 103. Di Gregorio Barletta G, Vittoria M, Lanzilli M, Petrillo C, Ricca E, & Isticato  
1159 R. CotG controls spore surface formation in response to the temperature of growth in  
1160 *Bacillus subtilis*. *Environ Microbiol.* 2022; 24: 2078-2088.
- 1161 104. Daniel RA, Errington J. Cloning, DNA sequence, functional analysis and  
1162 transcriptional regulation of the genes encoding dipicolinic acid synthetase required for  
1163 sporulation in *Bacillus subtilis*. *J Mol Biol.* 1993; 232: 468-83.
- 1164 105. Ramírez-Guadiana FH, Meeske AJ, Rodrigues CDA, Barajas-Ornelas RDC,  
1165 Kruse AC, Rudner DZ. A two-step transport pathway allows the mother cell to nurture  
1166 the developing spore in *Bacillus subtilis*. *PLoS Genet.* 2017b; 13: e1007015.
- 1167 106. Gao Y, Barajas-Ornelas RDC, Amon JD, Ramírez-Guadiana FH, Alon A, ...&  
1168 Rudner DZ. The SpoVA membrane complex is required for dipicolinic acid import  
1169 during sporulation and export during germination. *Genes Dev.* 2022; 36: 634-646.
- 1170 107. Tovar-Rojo F, Chander M, Setlow B, Setlow P. The products of the spoVA  
1171 operon are involved in dipicolinic acid uptake into developing spores of *Bacillus*  
1172 *subtilis*. *J Bacteriol.* 2002; 184: 584-587.
- 1173 108. Cabrera-Martinez RM, Tovar-Rojo F, Vepachedu VR, Setlow P. Effects of  
1174 overexpression of nutrient receptors on germination of spores of *Bacillus subtilis*. *J*  
1175 *Bacteriol.* 2003; 185: 2457-2464.
- 1176 109. Ghosh S, Scotland M, & Setlow P. Levels of germination proteins in dormant  
1177 and superdormant spores of *Bacillus subtilis*. *J Bacteriol.* 2012; 194: 2221-2227.
- 1178 110. Chen Y, Ray WK, Helm RF, Melville SB, & Popham DL. Levels of germination  
1179 proteins in *Bacillus subtilis* dormant, superdormant, and germinating spores. *PLoS One*,  
1180 2014; 9: e95781
- 1181 111. Corfe BM, Sammons RL, Smith DA, Mauël C. The gerB region of the *Bacillus*  
1182 *subtilis* 168 chromosome encodes a homologue of the gerA spore germination operon.  
1183 *Microbiol.* 1994; 140: 471-478.
- 1184 112. Behravan J, Chirakkal H, Masson A, Moir A. Mutations in the gerP locus of  
1185 *Bacillus subtilis* and *Bacillus cereus* affect access of germinants to their targets in  
1186 spores. *J Bacteriol.* 2000; 182:1987-1994.

- 1187 113. Feavers IM, Foulkes J, Setlow B, Sun D, Nicholson W, Setlow P, Moir A. The  
1188 regulation of transcription of the *gerA* spore germination operon of *Bacillus subtilis*.  
1189 Mol Microbiol. 1990; 4: 275-282.
- 1190 114. Amon JD, Artzi L, Rudner DZ. Genetic Evidence for Signal Transduction within  
1191 the *Bacillus subtilis* GerA Germinant Receptor. J Bacteriol. 2022; 204: e0047021.
- 1192 115. Abhyankar W, Pandey R, Ter Beek A, Brul S, de Koning LJ, & de Koster CG.  
1193 Reinforcement of *Bacillus subtilis* spores by cross-linking of outer coat proteins during  
1194 maturation. Food Microbiol. 2015; 45: 54-62.
- 1195 116. Paidhungat M, Setlow P. Role of ger proteins in nutrient and nonnutrient  
1196 triggering of spore germination in *Bacillus subtilis*. J Bacteriol. 2000; 182: 2513-2519.
- 1197 117. Paidhungat M, Ragkousi K, Setlow P. Genetic requirements for induction of  
1198 germination of spores of *Bacillus subtilis* by Ca(2+)-dipicolinate. J Bacteriol. 2001; 183:  
1199 4886-4893.
- 1200 118. Segev E, Smith Y, & Ben-Yehuda S. RNA dynamics in aging bacterial spores.  
1201 Cell. 2012; 148: 139-149.
- 1202 119. Bressuire-Isoard C, Broussolle V, & Carlin F. Sporulation environment  
1203 influences spore properties in *Bacillus*: evidence and insights on underlying molecular  
1204 and physiological mechanisms. FEMS Microbiol Rev. 2018; 42: 614-626.
- 1205 120. Rao L, Zhou B, Serruya R, Moussaieff A, Sinai L, & Ben-Yehuda S. Glutamate  
1206 catabolism during sporulation determines the success of the future spore germination.  
1207 iScience. 2022; 25: 105242.
- 1208 121. O'Brien T, & Campbell Jr LL. The nutritional requirements for germination and  
1209 out-growth of spores and vegetative cell growth of some aerobic spore forming bacteria.  
1210 J Bacteriol. 1957; 73: 522-525.
- 1211 122. Harwood CR and Cutting SM. Molecular Biological Methods for *Bacillus*.  
1212 Wiley, 1990.
- 1213 123. Schaeffer P, Millet J, Aubert J-P. Catabolic repression of bacterial sporulation.  
1214 Proc Natl Acad Sci USA. 1965; 54: 704-711.
- 1215 124. Arnaud M, Chastanet A, & Débarbouillé M. New vector for efficient allelic  
1216 replacement in naturally nontransformable, low-GC-content, gram-positive bacteria.  
1217 Appl Environ Microbiol. 2004; 70: 6887-6891.

- 1218 125. van Ooij C, Eichenberger P, Losick R. Dynamic patterns of subcellular protein  
1219 localization during spore coat morphogenesis in *Bacillus subtilis*. *J Bacteriol.* 2004; 186:  
1220 4441-8.
- 1221 126. Schindelin J, Arganda-Carreras I, Frise E, Kaynig V, Longair M, Pietzsch T, et  
1222 al. Fiji: an open-source platform for biological-image analysis. *Nat Methods.* 2012; 9:  
1223 676-682.
- 1224 127. Bechhofer DH, Oussenko IA, Deikus G, Yao S, Mathy N, et al. Analysis of  
1225 mRNA decay in *Bacillus subtilis*. *Methods Enzymol.* 2008; 447: 259–276.
- 1226 128. Redko Y, Aubert S, Stachowicz A, Lenormand P, Namane A, Darfeuille F, ... &  
1227 De Reuse H. A minimal bacterial RNase J-based degradosome is associated with  
1228 translating ribosomes. *Nucleic Acids Res.* 2013; 41: 288-301.
- 1229 129. Gilet L, Pellegrini O, Trinquier A, Tolcan A, Allouche D, Braun F, ... & Condon  
1230 C. Analysis of *Bacillus subtilis* Ribonuclease Activity In Vivo. In *RNA Remodeling*  
1231 *Proteins: Methods and Protocols 2020*; New York, NY: Springer US.
- 1232 130. Riesenman PJ, Nicholson WL. Role of the spore coat layers in *Bacillus subtilis*  
1233 spore resistance to hydrogen peroxide, artificial UV-C, UV-B, and solar UV radiation.  
1234 *Appl Environ Microbiol.* 2000; 66: 620-626.
- 1235 131. Theodorou I, Courtin P, Palussière S, Kulakauskas S, Bidnenko E, Péchoux C,  
1236 ... & Chapot-Chartier M-P. A dual-chain assembly pathway generates the high structural  
1237 diversity of cell-wall polysaccharides in *Lactococcus lactis*. *J Biol Chem.* 2019; 294:  
1238 17612-17625.

1239  
1240  
1241  
1242

## 1243 **FIGURE LEGENDS**

### 1244 **Fig 1. Rho is specifically expressed during *B. subtilis* sporulation.**

1245 (A) Rho expression in vegetative cells is limited to the exponential growth phase and  
1246 autoregulated. Kinetics of luciferase activity in *B. subtilis* WT  $P_{rho}$ -*luc* (empty circles) and RM  
1247  $P_{rho}$ -*luc* (filled-in circles) cells grown in rich medium LB. In this and other panels, the plain  
1248 dotted and solid lines represent growth curves of the Rho-proficient strains and *rho*-deletion  
1249 mutant (RM), respectively, measured by optical density OD<sub>600</sub>. (B) In the sporulation-inducing

1250 conditions, *rho* expression is additionally activated in stationary phase. Comparative analysis  
1251 of the luciferase activity in WT  $P_{rho}$ -*luc* cells grown in LB (brown circles) and in sporulation  
1252 medium DSM (blue circles). Activation of luciferase expression from the early sporulation  
1253 promoter *spoIIA* in the control WT  $P_{spoIIA}$ -*luc* cells grown in DSM (grey squares) marks the  
1254 initiation of sporulation. (C) In the sporulation-inducing conditions, the autoregulation of Rho  
1255 is weakened in stationary phase. Kinetics of luciferase activity in *B. subtilis* WT  $P_{rho}$ -*luc* (empty  
1256 blue circles) and RM  $P_{rho}$ -*luc* (filled-in blue circles) cells grown in sporulation medium DSM.  
1257 (D) Rho expression in the sporulation-inducing conditions correlates with the activation of  
1258 Spo0A. Comparative analysis of luciferase expression from  $P_{rho}$ -*luc* (blue circles) and  $P_{spo0A}$ -  
1259 *luc* (pink triangles) transcriptional fusions in WT (empty symbols) and RM (filled-in symbols)  
1260 cells grown in DSM. (E and F) Rho expression in stationary phase depends on the initiation of  
1261 sporulation. Kinetics of luciferase expression from  $P_{rho}$ -*luc* transcriptional fusions in WT cells  
1262 (blue circles) and the sporulation mutants (E): *spo0A* (orange circles) and *sigH* (grey circles);  
1263 and (F): *sigF* (red circles) and *sigE* (green circles). Measurements were taken every 5 minutes  
1264 after cells inoculation in media at optical density  $OD_{600} \sim 0.025$  (time point 0). For each strain,  
1265 plotted are the mean values of luminescence readings corrected for OD from four independent  
1266 cultures analyzed simultaneously. Each panel presents the simultaneously collected data. The  
1267 data in (C) and (D) and in (E) and (F) were obtained in two independent experiments. Each  
1268 strain and growth condition was tested at least three times. The results from the representative  
1269 experiment are presented.

1270 **Fig 2. Role of the read-through transcription in the *rho* expression during sporulation.** (A)  
1271 Schematic representation of gene organization and transcription within the *rho* locus of *B.*  
1272 *subtilis* chromosome. Arrow-shaped and flat rectangles indicate protein-coding genes and non-  
1273 coding RNA S-segments (Nicolas et al., 2012), respectively. Curved arrow-ended lines  
1274 represent promoters; their regulatory sigma factors are indicated. Straight dot-ended lines  
1275 represent intrinsic terminators. The underlying lines indicate the transcripts of the *rho* gene,  
1276 which were identified in (Nicolas et al., 2012); the transcript initiated at the known *rho*  
1277 promoter is bolded. The approximate size of the transcripts is shown. Small black rectangle  
1278 schematizes the 5' *rho*-specific riboprobe used in the Northern blot. (B) Cartoon of the insertion  
1279 of three intrinsic terminators at the end of *glpX* gene in the 3TER strain. (C) Northern blot  
1280 analysis of the *rho*-specific transcripts in the wild type (WT), and the mutant *sigH* and 3TER  
1281 strains during sporulation. Cells were grown in DSM and sampled during exponential growth  
1282 ( $OD_{600}$  0.5), the transition to stationary phase ( $OD_{600}$  1.0) and in stationary phase ( $OD_{600}$  1.8).

1283 Total RNA was extracted, processed and hybridized with the *rho*-specific riboprobe as  
1284 described in Materials and Methods. *Upper panel*. The *rho*-specific transcripts visualized by  
1285 Northern blotting. The arrows indicate the approximate size range of the transcripts. *Bottom*  
1286 *panel*. Ribosomal 16S and 25S RNAs stained with ethidium bromide were used to control the  
1287 equilibrium of the loaded RNA samples. (D) Suppression of the read-through transcription  
1288 inhibits *rho* expression in stationary phase. Kinetics of luciferase activity in *B. subtilis* WT  $P_{rho}$ -  
1289 *luc* (blue circles) and 3TER  $P_{rho}$ -*luc* (violet triangles) cells grown in the sporulation-inducing  
1290 DSM. (E and F) In the absence of read-through transcription, the residual expression of *rho* in  
1291 stationary phase still depends on sporulation. Kinetics of luciferase expression in 3TER  $P_{rho}$ -  
1292 *luc* strain (violet triangles) and its sporulation mutants (E): *spo0A* (orange triangles) and *sigH*  
1293 (grey triangles); and (F): *sigF* (red triangles) and *sigE* (green triangles) grown in DSM. The  
1294 data in (E) and (F) were obtained in the same experiment and are independent from (D). The  
1295 data were collected and processed as described in Fig 1. The experiments were reproduced at  
1296 least three times. The results from the representative experiment are presented.

1297 **Fig 3. The expression of *rho* in the forespore compartment of sporangium depends on**  
1298 **Sigma F.**

1299 The WT  $P_{rho}$ -*gfp* strain and its  $\Delta sigF$  and  $\Delta sigE$  mutant derivatives were induced for sporulation  
1300 by the resuspension method as described in Materials and Methods. Cells were sampled three  
1301 hours after resuspension in the nutrient-poor SM medium and observed by phase contrast  
1302 microscopy, and by epifluorescence illumination of GFP or membrane-affine dye in two  
1303 independent replicas. The right-hand cartoon depicts spatial GFP-mediated fluorescence in cells  
1304 with asymmetric septa.

1305 **Fig 4. Forespore-specific expression of *rho* depends on the activity of a genuine SigF-**  
1306 **dependent promoter.**

1307 (A and B) Sequence and structural elements of the SigA-dependent *rho* promoter reported by:  
1308 (A; Ingham et al., 1999) and (B; Nicolas et al., 2012). The -35 and -10 boxes are bolded and  
1309 colored in blue (A) and green (B). In (B), the upper blue lines indicate the relative position of  
1310 the *rho* promoter identified by (Ingham et al., 1999). (C) Sequence and structural elements  
1311 (bolded and colored in red) of putative SigF-dependent *rho* promoter identified in this analysis  
1312 as matching consensus sequences recognized by SigF-containing RNA polymerase (Wang et  
1313 al., 2006). The upper green lines indicate the relative position of the SigA-dependent *rho*  
1314 promoter identified by (Nicolas et al., 2012). The asterisk indicates a conserved thymine

1315 nucleotide in the -35 sequence of the SigF-dependent promoter subjected to mutagenesis. (D  
1316 and E) Mutations of the SigF-dependent *rho* promoter specifically inhibit *rho* expression in the  
1317 forespores. The wild type (WT) and 3TER cells bearing the non-modified P<sub>*rho*-gfp</sub> fusion and  
1318 WT P<sub>*rho*-gfp</sub> cells containing the indicated single-nucleotide mutations of putative SigF-  
1319 dependent *rho* promoter were induced for sporulation and analyzed for GFP-mediated  
1320 fluorescence as described in Materials and Methods and Fig 3. (D) Micrographs of typical cells  
1321 observed by phase contrast, epifluorescence illumination of GFP or membrane-affine dye. (E)  
1322 Average fluorescence intensities determined in predivisive cells and each compartments of  
1323 sporangia in each strain. Fluorescence intensity was determined as described in Materials and  
1324 Methods in two independent experiments. Bars represent standard deviation from the mean  
1325 values.

1326

1327 **Fig 5. The alteration of the spatiotemporal expression of *rho* affects the resistance**  
1328 **properties of mature spores.**

1329 Spores produced by WT and 3TER cells expressing *rho* from the non-modified promoters, their  
1330 mutant derivatives WT-mT/A and 3TER-mT/A inactivated for *rho* expression in the forespore  
1331 and RM cells expressing no Rho were analyzed for the levels of dipicolinic acid (A) and the  
1332 resistance to ultraviolet irradiation (B) as described in Materials and Methods. (A) Spore DPA  
1333 contents are normalized to the wild type level. The assay was reproduced ten times with two  
1334 independently prepared sets of five spores. Plotted are mean values from all measurements.  
1335 Statistical significance was estimated with a two-tailed t-test. The displayed p-value is as  
1336 follows: \*\*\*  $p \leq 0.001$ . (B) UV test was reproduced five times with one set of spores. The bars  
1337 represent standard deviation from the mean values.

1338

1339 **Fig 6. The alteration of the spatiotemporal expression of *rho* affects the morphology of**  
1340 **spores.**

1341 Thin section transmission electron micrographs of spores produced by cells differentially  
1342 expressing *rho*. White arrows indicate a thinner and less electron-dense outer coat in RM, 3TER  
1343 and 3TER-mT/A spores, which did not express *rho* in the forespores during maturation. Black  
1344 arrows indicate the detachment of outer and inner coats in RM, WT-mT/A and 3TER-mT/A  
1345 which did not express *rho* in the mother cells.

1346

1347 **Fig 7. Rho activity determines the revival properties of spores.**

1348 Spores produced by WT (blue triangles), RM (red squares), 3TER (brown crosses), WT-mT/A  
1349 (orange circles) and 3TER-mT/A (violet diamonds) cells were induced by the germinant L-  
1350 alanine (10mM) and analyzed for germination (A) and outgrowth in the nutrient-poor MS  
1351 medium (B) as described in Materials and Methods. (C) WT (filled-in blue triangles) and RM  
1352 (filled-in red squares) spores were compared for outgrowth in the nutrient-replenished MS  
1353 medium containing 0.5% casamino acids. The experiments were performed at least twice with  
1354 three independent sets of spores. Each experiment included up to six replicas of individual  
1355 suspensions of spores. The results of the representative experiment are plotted. The bars  
1356 represent standard deviation from the mean values.

1357

1358 **Fig 8. The wild-type rate of spore outgrowth requires the expression of *rho* during spore**  
1359 **morphogenesis and *de novo* after germination.**

1360 *B. subtilis*  $P_{spac-rho}$  cells expressing Rho protein from the IPTG-inducible promoter were  
1361 induced to sporulate in DSM in the absence (brown symbols) or presence (violet symbols) of  
1362 IPTG 100 $\mu$ M. The mature spores were purified and analyzed for germination with L-alanine  
1363 (A and B) and outgrowth in MS medium (C and D) in the absence (A, B and C; circles) or  
1364 presence of IPTG 100mM (B and D; diamonds). The WT (bleu triangles) and RM (red squares)  
1365 spores produced simultaneously with  $P_{spac-rho}$  spores were used to compare the germination in  
1366 (A) and outgrowth in (C and D). Of note, *rho* induction by IPTG (B): had no effect on the  
1367 germination rates of the both types of  $P_{spac-rho}$  spores, but (D): accelerated the outgrowth of  
1368 spores expressing *rho* during morphogenesis (violet diamonds) to the WT level. The  
1369 experiments were performed at least twice with two independent samples of the IPTG-induced  
1370 or non-induced  $P_{spac-rho}$  spores and included up to six replicas of individual suspensions of  
1371 spores The results of the representative experiment are plotted. The bars represent standard  
1372 deviation from the mean values.

1373

1374

1375 **Supporting information**

1376

1377 **S1 Fig. Induction of *Prho-gfp* expression in the forespore follows the progression of the**  
1378 **engulfment process.**

1379 Montage of fluorescent microscopy images (upper row: green channel; lower row: red channel)  
1380 of individual wild type cells bearing  $P_{rho-gfp}$  transcriptional fusion during the growth in DSM.  
1381 Cells were labeled with the red fluorescent Nile-Red dye and observed 2 hours after entering

1382 stationary phase (T2). Images are displayed from left to right following the progression of the  
1383 sporulation process, from predivisive to fully engulfed prespore state (red channel), to show  
1384 an increase of the fluorescence levels (green channel) in the prespore.

1385

1386 **S2 Fig. Inactivation of the SigF-dependent *rho* promoter inhibits sporulation-specific**  
1387 **expression of luciferase in 3TER  $P_{rho}$ -*luc* cells.**

1388 The mutational analysis of the SigF-dependent promoter of *rho* using luciferase was performed  
1389 in the 3TER genetic background to limit the interference of the read-through transcription.  
1390 3TER cells bearing a non-modified (violet triangles) or the point-mutated *mF-35T/A* (green  
1391 triangles) and *mF-35T/C* (orange triangles)  $P_{rho}$ -*luc* fusions were set to sporulate in DSM and  
1392 analyzed for luciferase activity as described in Fig 2. Of note, the mutation *mF-35T/A*  
1393 specifically decreases luciferase expression during sporulation, while the mutation *mF-35T/C*  
1394 has a global inhibitory effect (scaled differently in the graph). Nevertheless, the sporulation-  
1395 specific luminescence in 3TER *mF-35T/C*  $P_{rho}$ -*luc* is affected to a similar extent as in 3TER  
1396 *mF-35T/A*  $P_{rho}$ -*luc*.

1397

1398 **S3 Fig. Complete inactivation of *rho* has a maximal effect on sporulation efficiency. (A)**

1399 Cells were induced for sporulation by the resuspension method, sampled three hours after  
1400 resuspension, colored with lipid affine Mito-tracker red and analyzed by fluorescence  
1401 microscopy for the presence of asymmetric septum. The proportion of septum-containing cells  
1402 was determined by manual counting, in at least three fields of view and for a minimum of 600  
1403 cells per strain and per replica. Plotted are average proportions of septum-containing cells from  
1404 three experimental replica. The bars represent standard deviation from the mean values. (B and  
1405 C) After resuspension, cells were continuously propagated in a poor SM medium and analyzed  
1406 for the formation of heat-resistant spores at the indicated time (B) and overnight (20 hours) (C),  
1407 as described in Materials and Methods. Plotted are average proportions of the heat-resistant  
1408 spores from three independent experiments, two of which were performed in a prolongation of  
1409 microscopy analyses in (A). The bars represent standard deviation from the mean values.

1410

1411 **S4 Fig. Alteration of *rho* expression does not significantly affect the resistance of spores**  
1412 **to heat and lysozyme.**

1413 The purified spores of the wild type strain (WT), *rho*-deletion mutant (RM) and strains altered  
1414 for *rho* expression in the mother cell (3TER) or in the forespore (WT-mT/A) or in the two  
1415 compartments of sporangia (3TER-mT/A) were analyzed for the resistance to lysozyme (A and

1416 B) and heat (C). (A) Spores were activated as described in Materials and Methods, suspended  
1417 in TE buffer (10mM Tris-HCl, 1mM EDTA, pH 8.0) containing 10 mg/ml lysozyme (Fluka) at  
1418 OD<sub>600</sub> 0.2 and incubated at 37°C for 1 hour. (B) Spores were chemically treated to remove  
1419 spore coats as described in Materials and Methods. Decoated spores were suspended in 10mM  
1420 Tris-HCl (pH 8.0) at OD<sub>600</sub> 0.2 and treated with lysozyme (10 µg/ml, final concentration) for  
1421 10 and 20 minutes at 37°C. In (A) and (B), spore viability after lysozyme treatment was  
1422 established by plating spores from the treated and untreated samples at LB agar plates. (C) The  
1423 activated spores were heated at 90°C for the indicated time, plated at LB agar plates and  
1424 incubated at 37°C for 24 hours. The heat resistance of spores was calculated as a proportion of  
1425 viable colony-forming spores in heated and unheated samples. The same set of spores was used  
1426 in all experiments; spore samples in (B) originate from two independent decoating procedures.  
1427 The experiments were reproduced four times, and the established average values are presented  
1428 with the standard deviations of the mean (bars).

1429

1430 **S5 Fig. Rho inactivation does not affect UV-resistance of vegetative cells.**

1431 The wild type (WT, blue line) and *Δrho* (RM, red line) cells were grown in LB to OD<sub>600</sub> 0.5,  
1432 plated at LB-agar plates in serial dilutions and irradiated by ultraviolet light at the indicated  
1433 doses using the UV crosslinker as described in Materials and Methods. Cells were scored after  
1434 24h of incubation at 37°C. The experiment was reproduced twice with three culture samples  
1435 of each strain. Plotted are the mean values from two experiments.

1436

1437 **S6 Fig. Absence of Rho accelerates spore germination with different nutrient germinators.**

1438 Spores produced by WT (blue triangles), RM (red squares), 3TER (brown crosses), WT-mT/A  
1439 (orange circles) and 3TER-mT/A (violet diamonds) cells were induced for germination by (A)  
1440 the germinant AGFK (10 mM L-asparagine, 1mM D-glucose, 10mM KCl and 10 mM D-  
1441 fructose, final concentrations) or (B) L-valine (10mM). The experiments were performed twice  
1442 with two independent sets of spores. Each experiment included up to six replicas of individual  
1443 suspensions of spores. The results of the representative experiment are plotted. The bars  
1444 represent standard deviation of the mean values.

1445

1446 **S7 Fig. Absence of Rho does not affect viability of germinating spores.**

1447 The wild type WT (blue) and *rho*-minus RM (red) spore suspensions at OD<sub>600</sub> 0.1 were  
1448 activated and induced for germination by 10mM L-alanine as described in Materials and  
1449 Methods. Spore viability during germination was established by plating of spores in sequential

1450 dilutions at LB-agar plates at the indicated time after germinant addition. Plates were incubated  
 1451 at 37°C for 24h before the colonies counting. The experiment was reproduced twice with two  
 1452 independently prepared spore samples and included four replicas of each spore suspension. The  
 1453 results of the representative experiment are plotted. The bars represent standard deviation from  
 1454 the mean values.

1455

1456 **S8 Fig. Functional analysis of  $P_{spac-rho}$  transcriptional fusion.**

1457

1458 *B. subtilis* cells expressing *rho* from the IPTG-inducible promoter ( $P_{spac-rho}$ ) were incubated in  
 1459 LB medium in the presence of the indicated concentrations of IPTG to OD<sub>600</sub> 0.6 and analyzed  
 1460 for the levels of Rho protein in comparison with wild-type cells (WT) by Western blot with the  
 1461 specific anti-Rho<sup>Bs</sup> anti-serum as described in Materials and Methods. Protein equilibrium  
 1462 between the loaded samples was controlled by Bradford assay and visualization of Mbl protein  
 1463 by anti-Mbl antibodies as described in (Bidnenko et al., 2023).

1464

1465 **S1 Table. Differential expression analysis of genes from the “Sporulation” lifestyle**  
 1466 **category in stationary  $\Delta rho$  vs. stationary WT *B. subtilis* cells (compiled from S3 Table,**  
 1467 **Bidnenko et al., 2023).**

1468 **S2 Table. Strains and plasmids used in the analysis.**

1469 **S3 Table. Oligonucleotides used for strains construction.**

1470

1471

1472 **S2 Table. Strains and plasmids used in this study.**

Strains	Genotype (resistance)	Source or reference
BSB1	<i>B. subtilis</i> 168 <i>trp</i> <sup>+</sup>	Nicolas <i>et al.</i> , 2012
BRL1	BSB1 $\Delta rho::phleo$ ( <i>phleo</i> <sup>R</sup> )	Bidnenko <i>et al.</i> , 2017
BRL111	BSB1 $P_{spoIIA-luc}$ ( <i>Cm</i> <sup>R</sup> )	Bidnenko <i>et al.</i> , 2017
BRL116	BSB1 $P_{spo0A-luc}$ ( <i>Cm</i> <sup>R</sup> )	Bidnenko <i>et al.</i> , 2017
BRL118	$\Delta rho::phleo P_{spo0A-luc}$ ( <i>Cm</i> <sup>R</sup> )	Bidnenko <i>et al.</i> , 2017
BRL871	BSB1 $P_{rho-luc}$ ( <i>Cm</i> <sup>R</sup> )	This study
BRL880	$\Delta rho::phleo P_{rho-luc}$ ( <i>phleo</i> <sup>R</sup> <i>Cm</i> <sup>R</sup> )	This study
ABS549	PY79 $\Delta spo0A::tet$ ( <i>Tet</i> <sup>R</sup> )	Chastanet <i>et al.</i> , 2010
BKK00980	<i>B. subtilis</i> 168 <i>trpC2 sigH::km</i> ( <i>Km</i> <sup>R</sup> )	Koo <i>et al.</i> , 2017
BRL877	BSB1 $spo0A::tet P_{rho-luc}$ ( <i>Tet</i> <sup>R</sup> <i>Cm</i> <sup>R</sup> )	This study
BRL898	BSB1 $sigH::km P_{rho-luc}$ ( <i>Km</i> <sup>R</sup> <i>Cm</i> <sup>R</sup> )	This study
RL1265	$sigF::km (spoIIAC\Delta::km)$	Fawcett <i>et al.</i> , 2000

EU8701	<i>sigE::erm (spoIIIGBA::erm)</i>	Kenney and Moran, 1987
MO1780	<i>sigE::tet (spoIIIGABA::tet)</i>	Guérout-Fleury <i>et al.</i> , 1996
BRL878	BSB1 <i>sigE::erm P<sub>rho</sub>-luc</i> (Em <sup>R</sup> Cm <sup>R</sup> )	This study
BRL879	BSB1 <i>sigF::km P<sub>rho</sub>-luc</i> (Km <sup>R</sup> Cm <sup>R</sup> )	This study
BRL894	BSB1 <i>P<sub>rho</sub>-gfp</i> (Sp <sup>R</sup> )	This study
BRL956	BSB1 <i>sigE::tet P<sub>rho</sub>-gfp</i> (Tet <sup>R</sup> Sp <sup>R</sup> )	This study
BRL957	BSB1 <i>sigF::km P<sub>rho</sub>-gfp</i> (Km <sup>R</sup> Sp <sup>R</sup> )	This study
BRL1111	3TER <i>P<sub>rho</sub>-luc</i> (Cm <sup>R</sup> )	This study
BRL1119	3TER <i>-35mT/C P<sub>rho</sub>-luc</i> (Cm <sup>R</sup> )	This study
BRL1165	3TER <i>-35mT/A P<sub>rho</sub>-luc</i> (Cm <sup>R</sup> )	This study
BRL1159	3TER <i>P<sub>rho</sub>-gfp</i> (Sp <sup>R</sup> )	This study
BRL1144	BSB1 <i>-35mT/C P<sub>rho</sub>-gfp</i> (Sp <sup>R</sup> )	This study
BRL1172	BSB1 <i>-35mT/A P<sub>rho</sub>-gfp</i> (Sp <sup>R</sup> )	This study
BRL1175	3TER <i>spo0A::tet P<sub>rho</sub>-luc</i> (Tet <sup>R</sup> Cm <sup>R</sup> )	This study
BRL1176	3TER <i>sigH::km P<sub>rho</sub>-luc</i> (Km <sup>R</sup> Cm <sup>R</sup> )	This study
BRL1177	3TER <i>sigE::tet P<sub>rho</sub>-luc</i> (Tet <sup>R</sup> Cm <sup>R</sup> )	This study
BRL1178	3TER <i>sigF::km P<sub>rho</sub>-luc</i> (Km <sup>R</sup> Cm <sup>R</sup> )	This study
BRL1130	3TER	This study
BRL1185	BSB1 <i>-35mT/A</i>	This study
BRL1194	3TER <i>-35mT/A</i>	This study
BRL1300	BSB1 <i>rho.ΩP<sub>spac</sub>-rho</i> (Em <sup>R</sup> )	This study
<b>Plasmids</b>		
pUC18Cm-luc	Cm <sup>R</sup> , Amp <sup>R</sup>	Mirouze <i>et al.</i> , 2011
pCVO119	Sp <sup>R</sup> Amp <sup>R</sup>	Van Ooij <i>et al.</i> , 2004
pMAD	Em <sup>R</sup> , Amp <sup>R</sup>	Arnaud <i>et al.</i> , 2004
pMUTIN4	Em <sup>R</sup>	Vagner <i>et al.</i> , 1998
pET28a	Km <sup>R</sup>	Novogen
pBRL862	Cm <sup>R</sup> , Amp <sup>R</sup> ; used to construct BRL871 ( <i>P<sub>rho</sub>-luc</i> )	This study
pBRL893	Sp <sup>R</sup> Amp <sup>R</sup> ; used to construct BRL894 ( <i>P<sub>rho</sub>-gfp</i> )	This study
pBRL1107	Cm <sup>R</sup> , Amp <sup>R</sup> ; used to construct BRL1111 (3TER <i>P<sub>rho</sub>-luc</i> )	This study
pBRL1150	Sp <sup>R</sup> Amp <sup>R</sup> ; used to construct BRL1159 (3TER <i>P<sub>rho</sub>-gfp</i> )	This study
pBRL1116	Cm <sup>R</sup> , Amp <sup>R</sup> ; used to construct BRL1119 (3TER <i>-35mT/C P<sub>rho</sub>-luc</i> )	This study
pBRL1162	Cm <sup>R</sup> , Amp <sup>R</sup> ; used to construct BRL1165 (3TER <i>-35mT/A P<sub>rho</sub>-luc</i> )	This study
pBRL1141	Sp <sup>R</sup> Amp <sup>R</sup> ; used to construct BRL1144 ( <i>-35mT/C P<sub>rho</sub>-gfp</i> )	This study
pBRL1164	Sp <sup>R</sup> Amp <sup>R</sup> ; used to construct BRL1172 ( <i>-35mT/A P<sub>rho</sub>-gfp</i> )	This study
pBRL1108	Em <sup>R</sup> , Amp <sup>R</sup> ; used to construct BRL1130 (3TER)	This study
pBRL1174	Em <sup>R</sup> , Amp <sup>R</sup> ; used to construct BRL1185 (BSB1 <i>-35mT/A</i> )	This study
pBRL1180	Em <sup>R</sup> , Amp <sup>R</sup> ; used to construct BRL1194	This study

	(3TER -35mT/A)	
pMutin4rho	Em <sup>R</sup> , Amp <sup>R</sup> ; used to construct BRL1300 (rhoΩP <sub>spac</sub> -rho)	This study
pETRho	Km <sup>R</sup> ; pET28a-rho	This study

1473

- 1474 1. Mirouze N, Prepiak P, & Dubnau D. Fluctuations in spo0A transcription control rare  
1475 developmental transitions in Bacillus subtilis. PLoS Genet. 2011. 7: e1002048.
- 1476 2. Van Ooij, C., Eichenberger, P., & Losick, R. (2004). Dynamic patterns of subcellular  
1477 protein localization during spore coat morphogenesis in Bacillus subtilis. *Journal of*  
1478 *bacteriology*, 186(14), 4441-4448.
- 1479 3. Arnaud M, Chastanet A, Débarbouillé M. New vector for efficient allelic replacement  
1480 in naturally nontransformable, low-GC-content, Gram-positive bacteria. Appl Environ  
1481 Microbiol. 2004; 70: 6887-6891. doi:10.1128/AEM.70.11.6887-6891.2004
- 1482 4. Vagner, V., Dervyn, E., & Ehrlich, S. D. (1998). A vector for systematic gene  
1483 inactivation in Bacillus subtilis. *Microbiology*, 144(11), 3097-3104.
- 1484 5. Chastanet, A., Vitkup, D., Yuan, G. C., Norman, T. M., Liu, J. S., & Losick, R. M.  
1485 (2010). Broadly heterogeneous activation of the master regulator for sporulation in  
1486 Bacillus subtilis. *Proceedings of the National Academy of Sciences*, 107(18), 8486-  
1487 8491.
- 1488 6. Fawcett, P., Eichenberger, P., Losick, R., & Youngman, P. (2000). The transcriptional  
1489 profile of early to middle sporulation in Bacillus subtilis. *Proceedings of the National*  
1490 *Academy of Sciences*, 97(14), 8063-8068.
- 1491 7. Guérout-Fleury, A. M., Frandsen, N., & Stragier, P. (1996). Plasmids for ectopic  
1492 integration in Bacillus subtilis. *Gene*, 180(1-2), 57-61.
- 1493 8. Kenney, T. J., & Moran Jr, C. P. (1987). Organization and regulation of an operon that  
1494 encodes a sporulation-essential sigma factor in Bacillus subtilis. *Journal of*  
1495 *bacteriology*, 169(7), 3329-3339.

1496

1497 **S3 Table. Oligonucleotides used for strains construction**

Oligonucleotide	Sequence (5' -> 3')
glpXBam *	CACGCTTCTGgATcCTCCTGACATG
veb738 **	TATGTTTTTGGCGTCTTCCATAAAAACACCACGCTTTTC
lucintrev	CAATCAGAGTGCTTTTGGCGAAG

veb739	ATGGAAGACGCCAAAAACATA
veb734	CTAGACCCGGGGATCTCTG
veb735	TCTAGAGCAACGTTCTTGC
veb797 **	<u>GCAAGAACGTTGCTCTAGACAAACAGAAAAAGCGGGTG</u>
veb798 **	<u>CAGAGATCCCCGGGTCTAGTTATGGACGGATTACAAGATTGG</u>
veb742 **	<u>GTTCTTCTCCTTTACTCATAAAAAACACCACGCTTTTC</u>
veb741	<i>acgcgtcgac</i> TTATTTGTATAGTTCATCCATG
veb740	ATGAGTAAAGGAGAAGAAC
veb802 ***	<u><b>c</b>AATTTTTT</u> GAAATAAGGTAAAAATAAAG
veb803	TTCAACTGAAATAAGGTTTTGAC
veb805 ***	<u><b>a</b>AATTTTTT</u> GAAATAAGGTAAAAATAAAG
veb795	CTTGG <i>Atcc</i> TAGTTGATCGGTCTC
veb796	TGGA <i>Att</i> CGCTGACGGTTATC
veb808	CTCTGAACATGTCATCTGCTGC
veb806	TGA <i>g</i> GATCCGGATAAAGTGGCG
veb807	GCAGCAGATGACATGTTTCAGAG
veb880	GGGTGGAATTCTTACCGATAGAAG
veb596	<i>cgcgctcgac</i> TTACCTTCTTGCAGATGATAG
veb599	<i>gatccat</i> ATGAAAGACGTATCTATTTCTC
YRH1****	<u>CTAATACGACTCACTATAGGAGACAGGAATCCGAAACCTTCAG</u>
YRH2	TCTCCTATTACAGCAAACCTGAC

1498

1499 \* Here and thereafter, the modified nucleotides are in small characters and the recognition  
1500 sites of the endonucleases are in italics.

1501 \*\* Sequences complementary to other oligonucleotides are underlined

1502 \*\*\* The 5'-terminal nucleotides creating the mutations are bolded and underlined.

1503 \*\*\*\* T7 promoter sequence is underlined.

1504

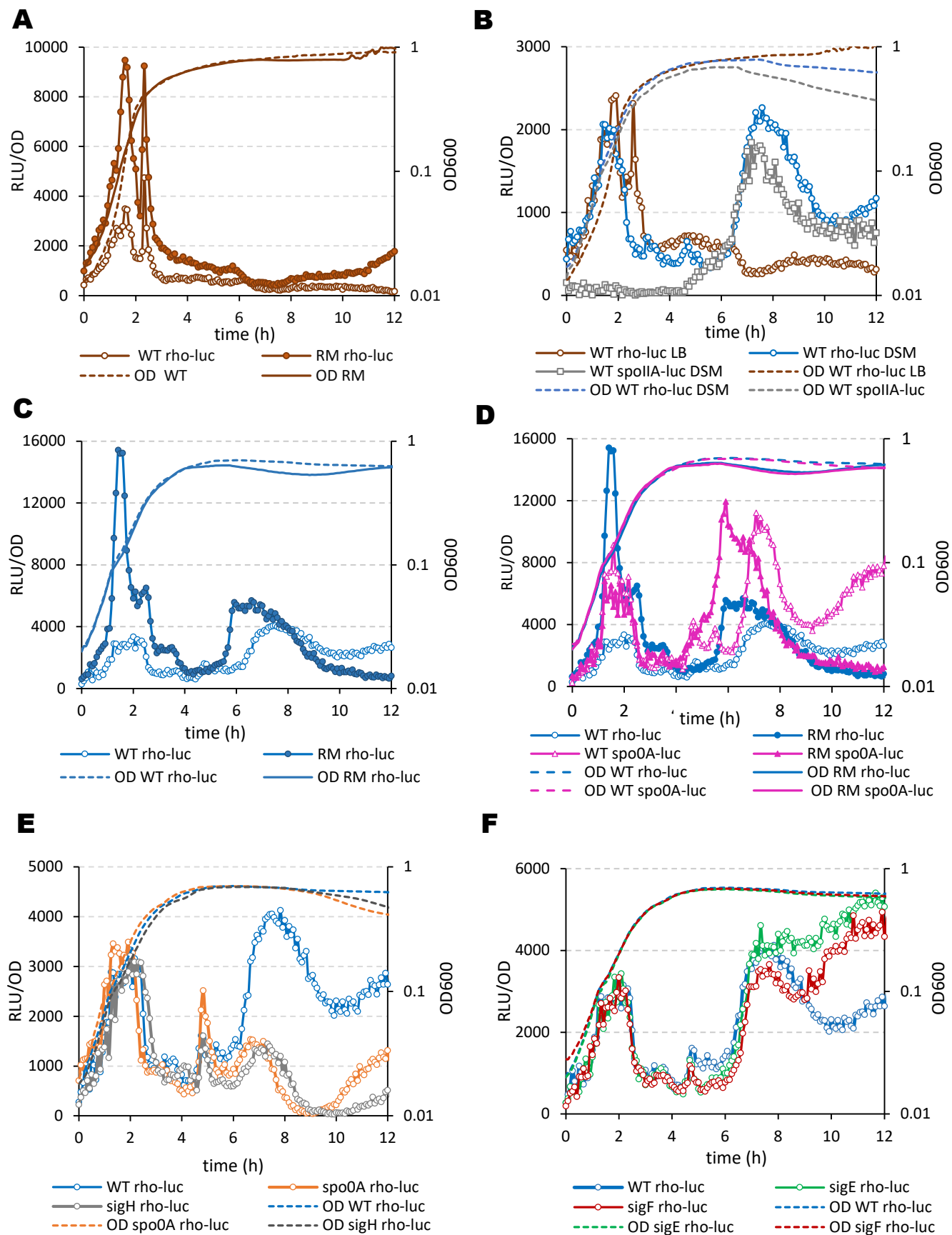


Fig 1

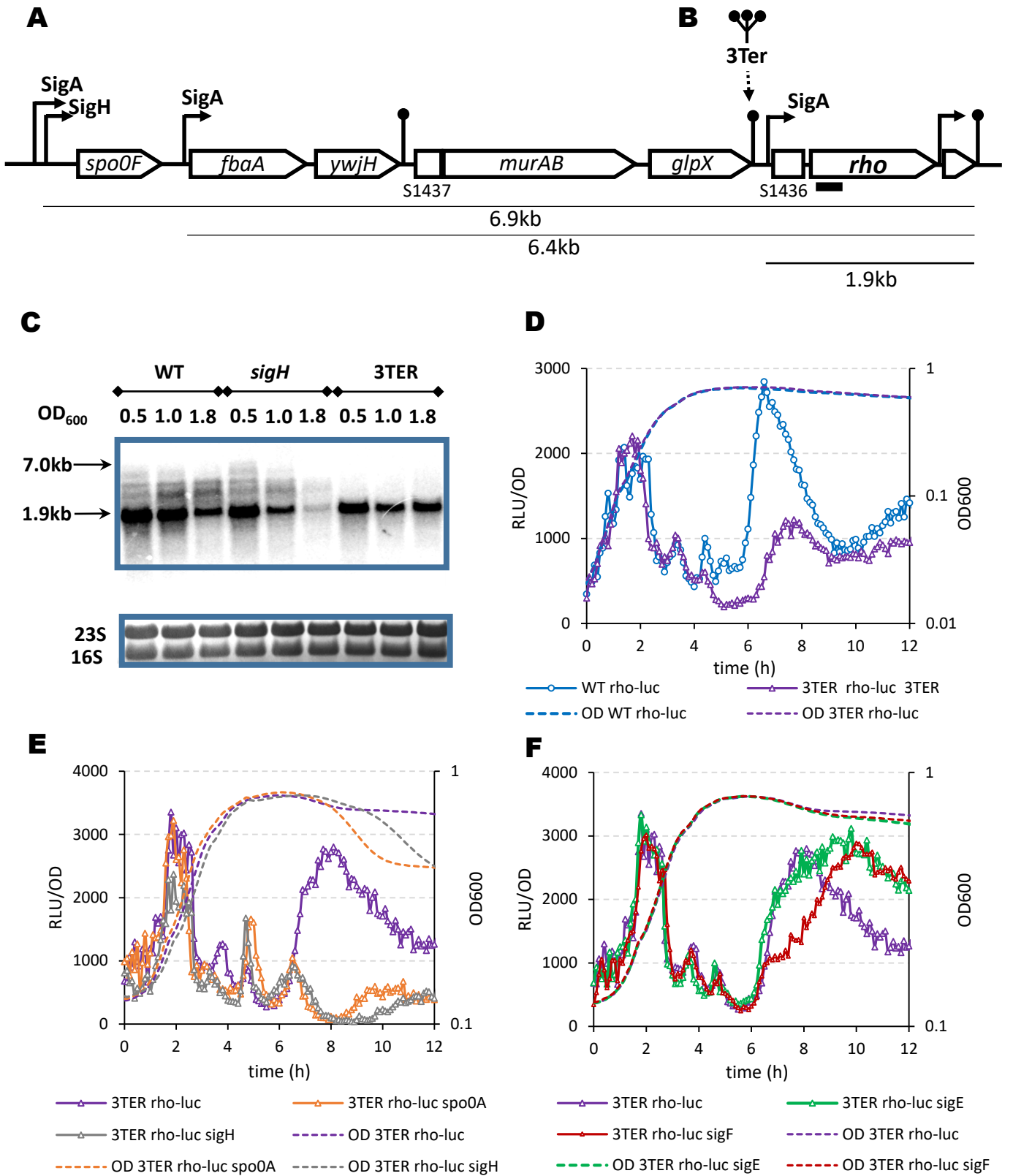


Fig 2

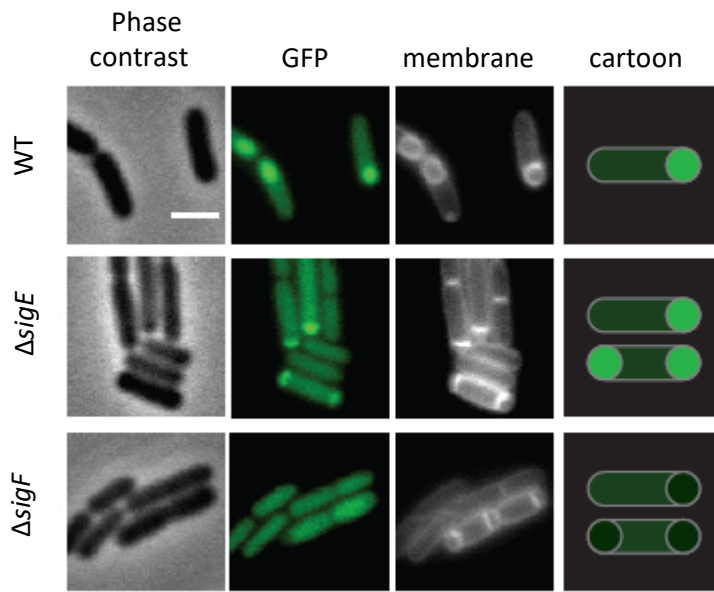


Fig 3

**A** tcagTGAATaatttttgaataaggTAAAAAtaaagagtgtgc  
 -35 -10

**B** tcAGTTGaataatttttgaaaTAAGGTAAAAATAAAGAGTGctgc  
 -35 -10

**C** tcagttGaATAaatttttgaataaGGTAAAAATAaagagtgtgc  
 -35 -10  
 \*  
 14 bp A/T rich spacer

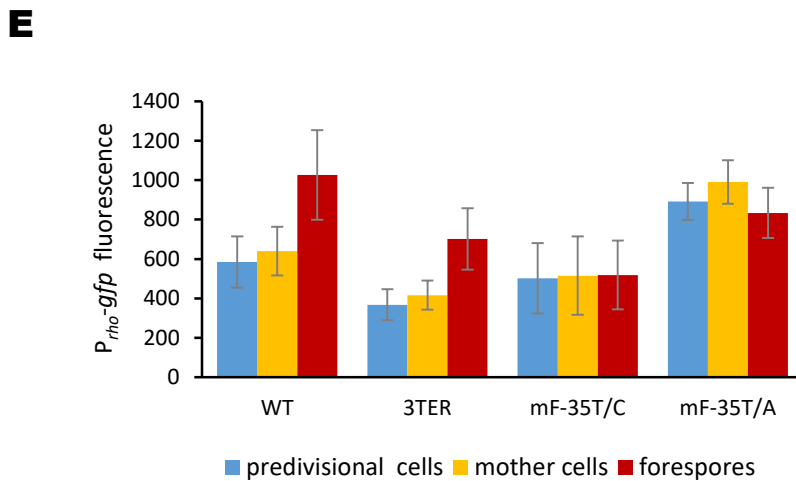
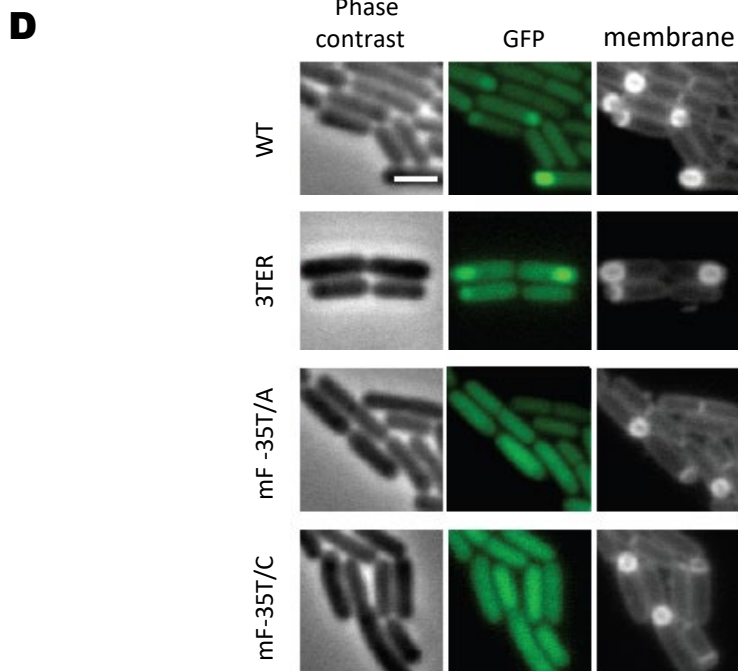


Fig 4

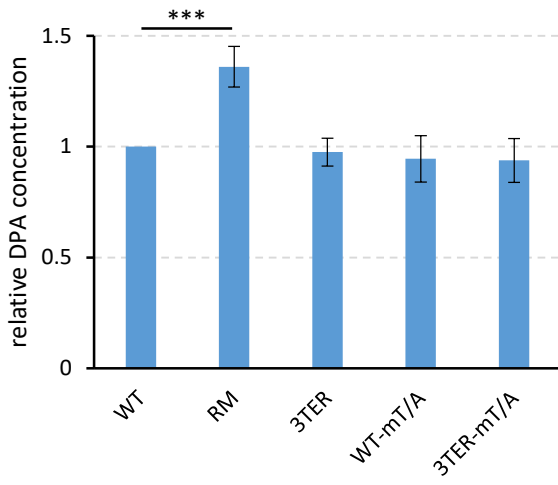
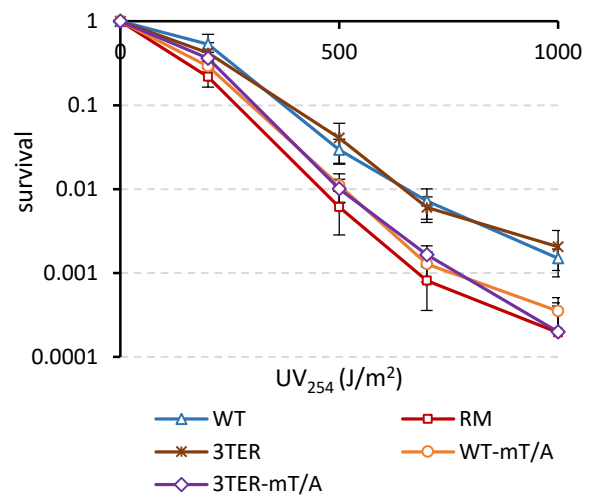
**A****B**

Fig 5

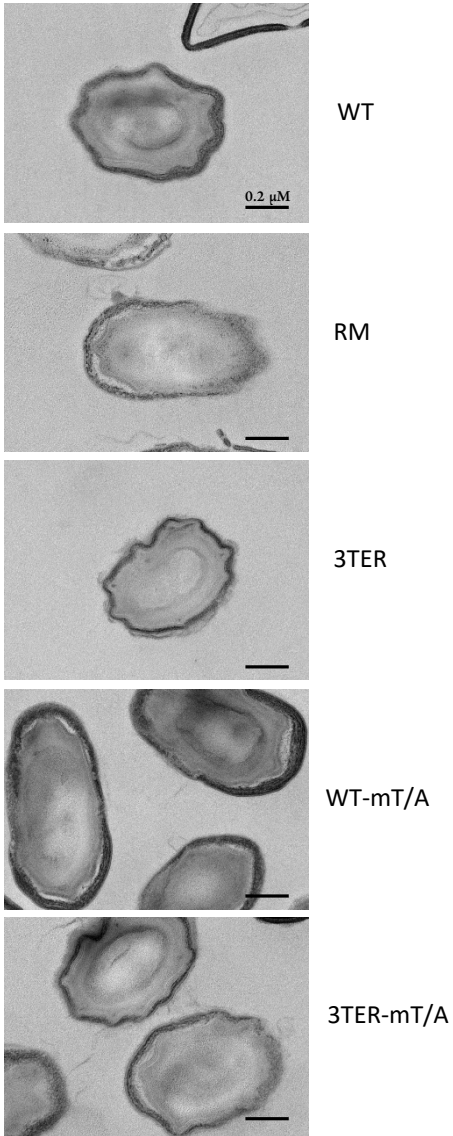


Fig 6

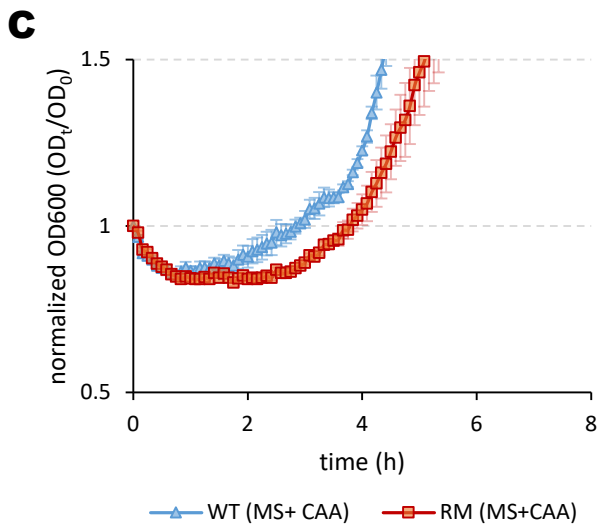
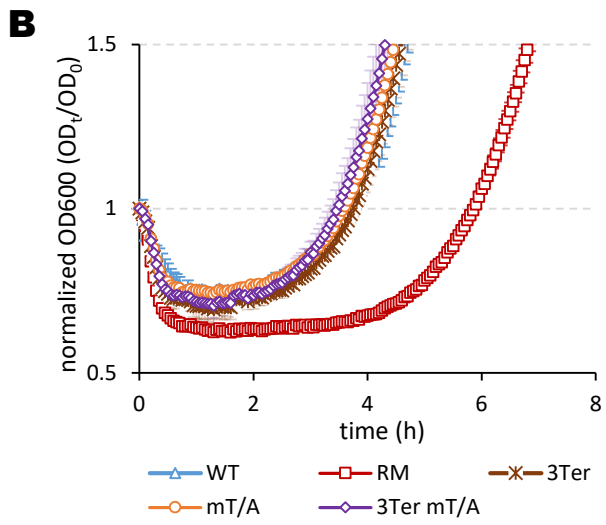
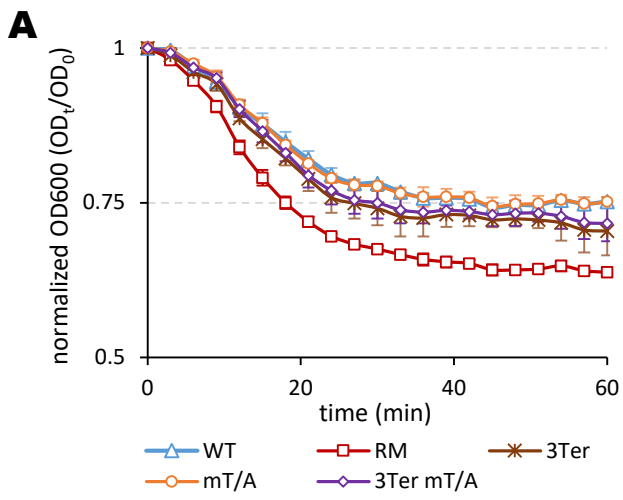


Fig 7

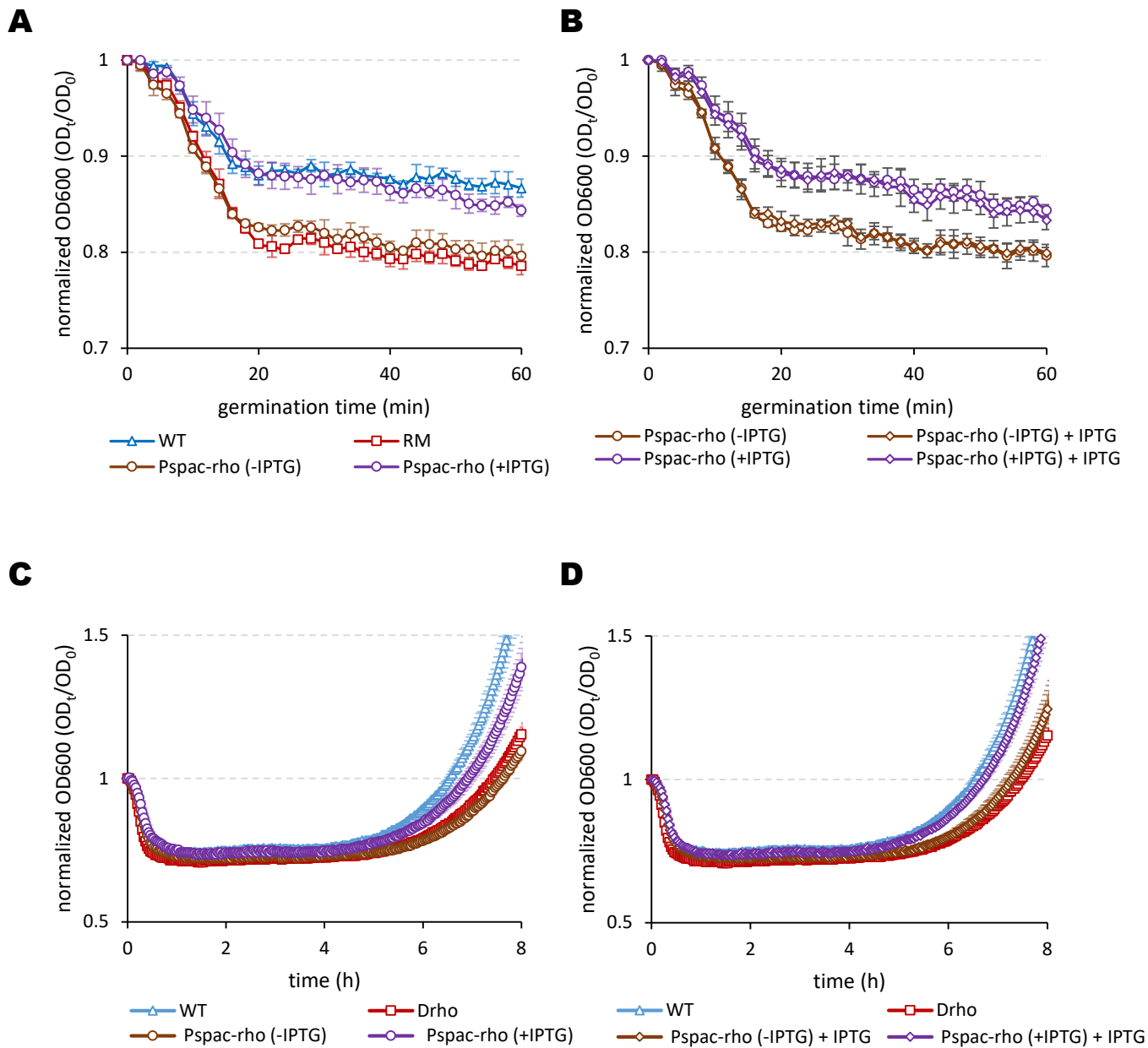
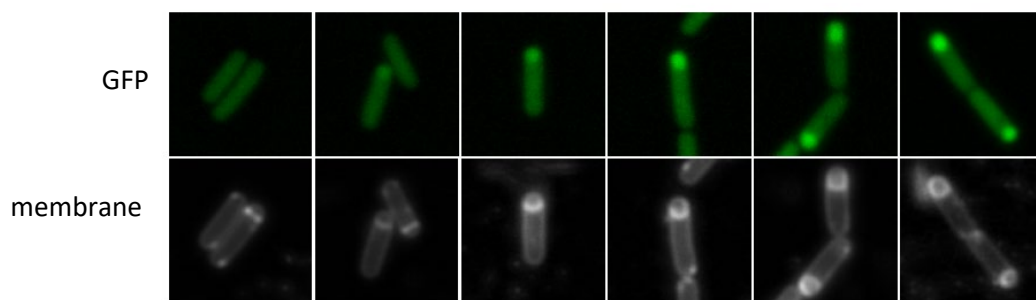
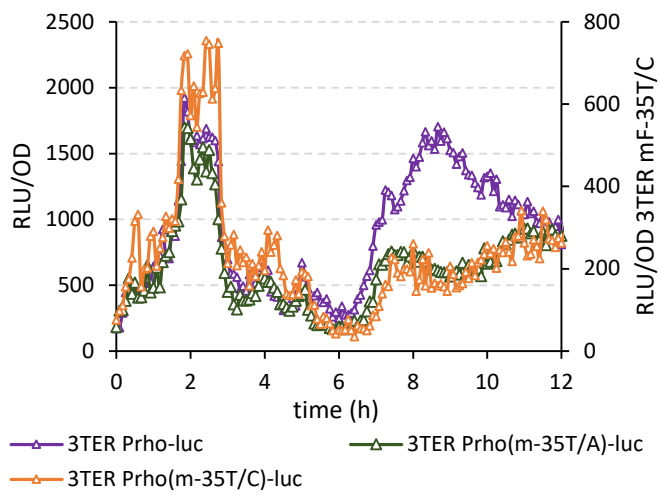


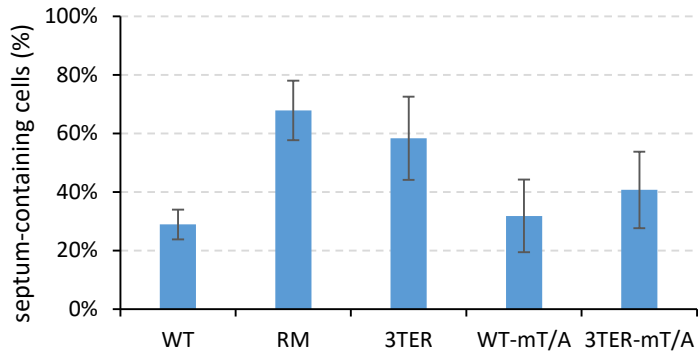
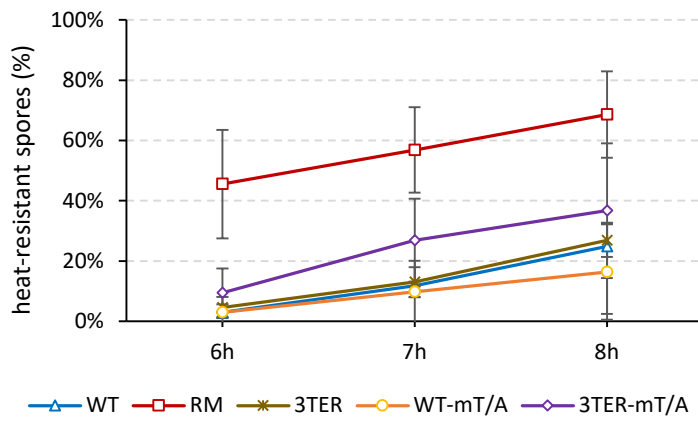
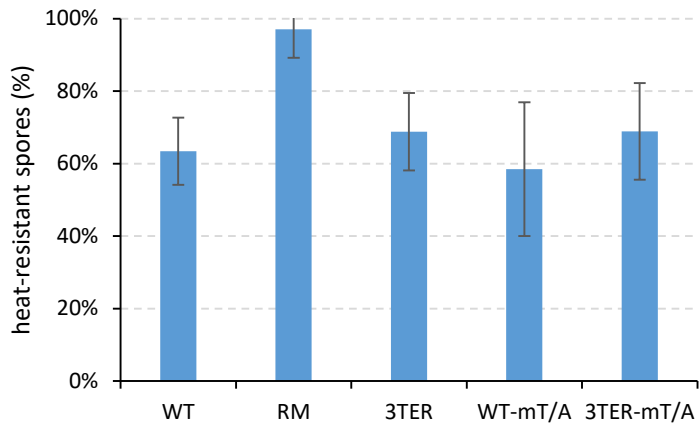
Fig 8



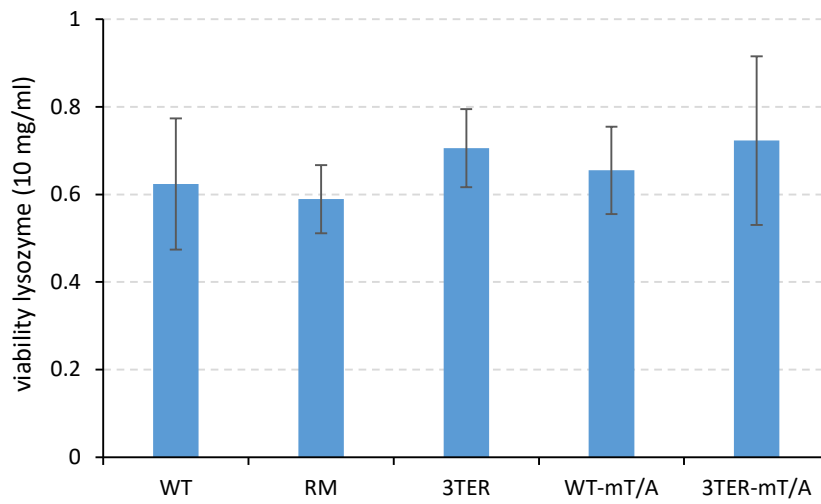
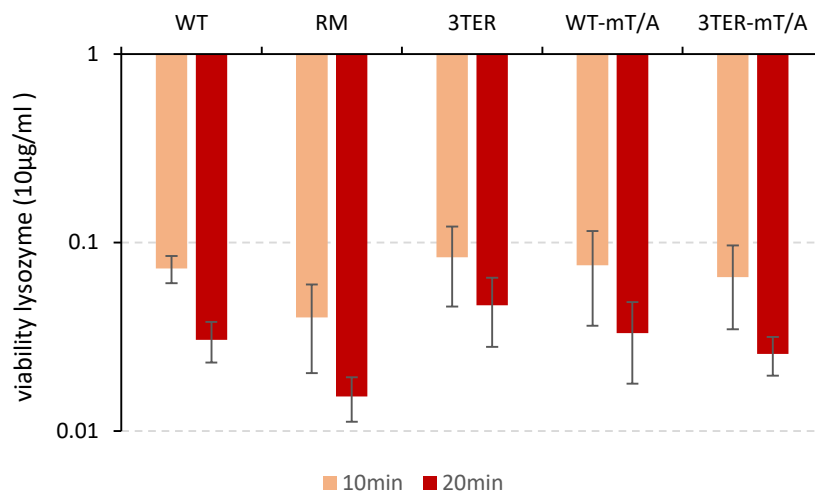
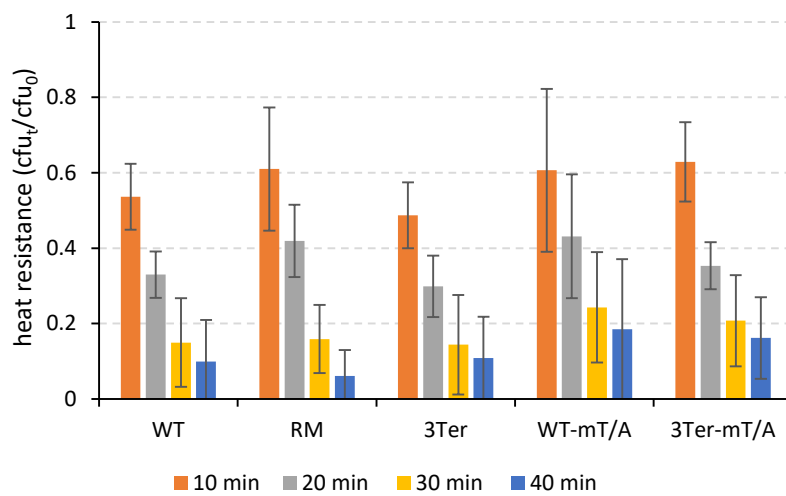
S1 Fig



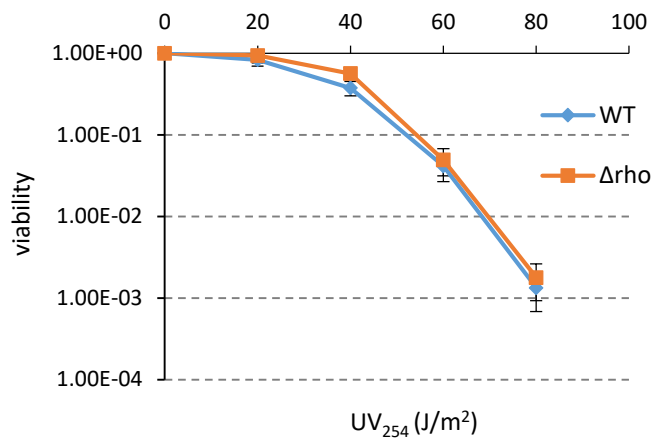
S2 Fig

**A****B****C**

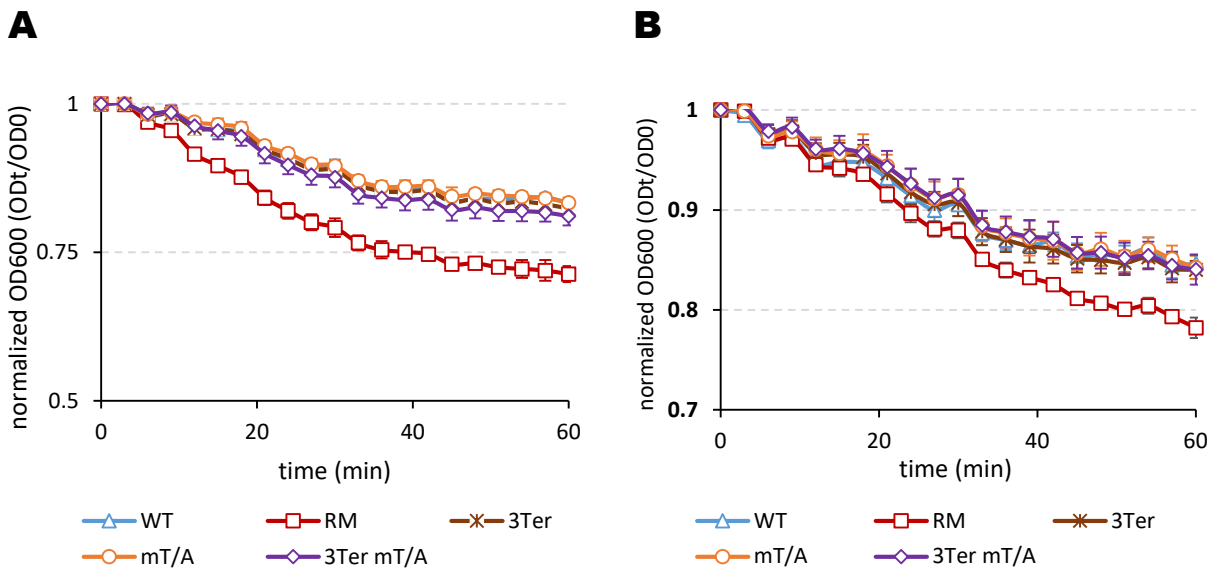
S3 Fig

**A****B****C**

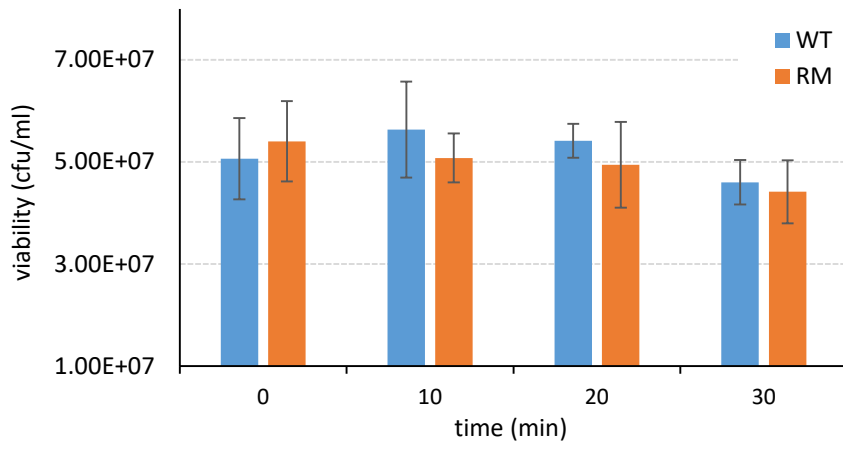
S4 Fig



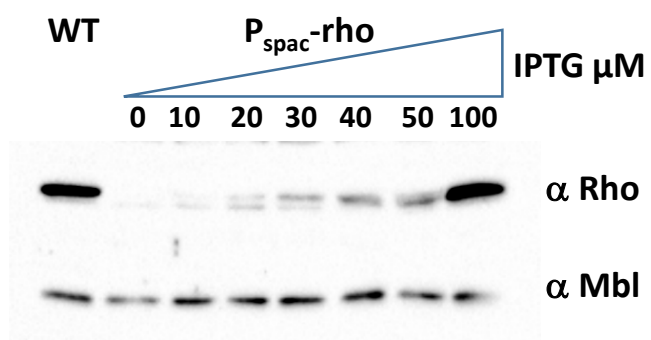
S5 Fig



S6 Fig



S7 Fig



S8 Fig